Attribution of surface ozone to NO$_x$ and VOC sources during two different high ozone events

Aurelia Lupaşcu[1], Noelia Otero[1,a], Andrea Minkos[2], and Tim Butler[1,3]

[1]Institute for Advanced Sustainability Studies (IASS), Potsdam, 14467, Germany
[2]German Environment Agency, 06844 Dessau-Roßlau, Germany
[3]Freie Universität Berlin, Institut für Meteorologie, Berlin, Germany
[a]now at: Oeschger Centre for Climate Change Research (OCCR), Bern, Switzerland

Correspondence: A.Lupascu (Aura.Lupascu@iass-potsdam.de)

Abstract. Increased tropospheric ozone (O$_3$) and high temperatures affect human health during heat waves. Here, we perform a source attribution that considers separately the formation of German surface ozone from emitted NO$_x$ and VOC precursors during two peak ozone events that took place in 2015 and 2018 which were associated with elevated temperatures. Results showed that the peak ozone concentrations can be primarily attributed to nearby emissions of anthropogenic NO$_x$ (from Germany and immediately neighboring countries) and biogenic VOC. Outside of these high ozone episodes, baseline ozone concentrations are attributed primarily to long-range transport, with ozone due to remote anthropogenic NO$_x$ emissions and methane oxidation adding to the tropospheric ozone background. We show that a significant contribution to modeled O$_3$ coming from German NO$_x$ or VOC emissions occurs mostly in southern Germany, emphasizing that the production of ozone depends on the local interplay among NO$_x$ and VOC precursors. Shipping activities in the Baltic and North Seas have a large impact on ozone predicted in coastal areas, yet a small amount of ozone from these sources can also be seen far inland, showing the importance of transported ozone on pollution levels. We have also shown that changes in circulation patterns during the peak O$_3$ episodes observed in Germany during the 2015 and 2018 heatwaves can affect the contribution of different NO$_X$ emission sources to total O$_3$, thus the possible influence of multiple upwind source regions should be accounted for when mitigation strategies are designed. Our study also highlights the good correlation between ozone coming from German biogenic VOC emissions and total ozone, although the diurnal variation in the ozone coming from biogenic sources is not dominated by the diurnal variation in biogenic emissions, and the peaks of ozone from biogenic sources are disconnected from local emission peaks. This suggests that the formation of O$_3$ from local German biogenic VOC emissions is not the sole factor that influences the ozone formation and other meteorological and chemical processes affect the diel variation of ozone having a biogenic origin. Overall, this study helps to understand the importance of a source attribution method to understand the sources of O$_3$ in Germany and can be a useful tool that will help to design effective mitigation strategies.

1 Introduction

Increased concentrations of ground-level ozone can harm humans and vegetation, especially during hot summer days (Sillmann et al., 2021). As shown by Analitis et al. (2014), the heatwave effect combined with the high ozone episodes is associated with an increase in mortality. Recent IPCC assessment reports (2012, 2018) associate an increase in the occurrence of extreme heatwave episodes with an increase in socioeconomic costs, and with an increase in ozone concentrations that cause morbidity from other diseases.

Several well-documented heatwaves associated with high ozone concentrations were registered over central and western Europe such as August 2003 (i.e., Vautard et al., 2005, Vieno et al., 2010) and July 2006 (i.e. Struzewska and Kaminski, 2008). Vautard et al. (2005) studied the 2003 heatwave using the CHIMERE model that reproduced very well the high observed ozone concentration at European monitoring stations. Struzewska and Kaminski (2008) have identified three independent factors that influence the level of photochemical pollution, such as the circulation patterns, the geographical location, and the intensity of anthropogenic nitrogen oxides (NO_x) emissions. Many studies showed that the main meteorological factor which drives high ozone pollution episodes is the temperature (i.e., Lin et al., 2001, Jacob and Winner, 2009, Porter et al., 2015, Pusede et al., 2015, and references therein; Otero et al., 2016, and references therein). Schnell and Prather (2017) showed that extreme events of ozone and temperature over North America often overlap, although consistent offsets in space and in time are occurring, most likely due to advection of emitted precursors.

During the last decades, global and regional chemical models were used to simulate the enhanced ozone concentrations associated with heatwaves (i.e., Guerova and Jones, 2007, Ordonez et al., 2010), as well as future high ozone episodes (Shen et al., 2016). Meehl et al. (2018) used a model simulation for a present-day climate and showed that during heatwave days the surface ozone enhancement exceeds 10 ppb over Europe compared to non-heatwave days. Chemical transport models (CTMs) are an important tool for the simulation of transport and transformation of gases and to study the relationship between meteorology and high air pollution episodes. More recent developments of CTMs enabled their capacity to tag the emissions by source (e.g., Grewe et al., 2017, Butler et al., 2018, 2020a, Lupașcu and Butler, 2019, Mertens et al., 2020); hence they can help to identify the main precursor sources contributing to ozone peaks.

Several studies have quantified the contribution of long-range transport vs local emissions impact on summer peak ozone in Europe. Jonson et al. (2018) showed that, for most of the models used in their inter-comparison study except for the model CHASER_re1 in summer, the contribution to European seasonal mean ozone levels is larger for regions from outside Europe than the contribution from European sources. Pay et al. (2019) showed that the imported ozone is the largest contributor to the ground level high ozone concentrations registered in Spain in July 2012. Lupașcu and Butler (2019) indicated that the local sources (precursors emitted within receptor regions) explain up to 35% of modeled daily maximum 8-hour average ozone (MDA8 O_3) in several receptor regions, while the remote sources accounted for 11% to 45% of the total surface ozone. Their work also showed the importance of locally emitted NOx precursors for the ozone metrics that are especially influenced by high values of ozone, such as MDA8 O_3, AOT40, W126, and 95th percentile.

Methane (CH_4) oxidation explains a large part of the ozone formation in the troposphere. Wang and Jacob (1998) showed that the historic increase of global methane emissions and its subsequent oxidation led, among other causes, to the increase of tropospheric ozone concentrations, but this increase depends on the local availability of OH radical. Turnock et al. (2018, 2019) showed that the reduction of CH_4 is a key factor for controlling the increase of future surface ozone. West and Fiore (2005) analyzed the advantages of low ozone due to methane emission reductions on agriculture, forest management, and human health and they found that the monetized global benefits would justify cutting the methane emissions by ~17%. In addition, Fiore et al. (2008) showed that the CH_4 oxidation contributes ~20% to the annual mean MDA8 O_3 at nearly all US MDA8 O_3 surface locations since the pre-industrial era, while Butler et al. (2020a) indicated that CH_4 oxidation explains 35% of their simulated global average tropospheric ozone burden.

Biogenic volatile organic compound (BVOC) emissions contribute strongly to the formation of ozone (e.g., Fiore et al., 2011, Curci et al., 2009, Qu et al., 2013, Tagaris et al., 2014, Zhang et al., 2017). Among them, isoprene is the main component. Biogenic isoprene emissions depend on multiple environmental drivers such as temperature, solar radiation, plant water stress, ozone, CO_2 concentrations, and land cover. Although Simpson et al. (1995) showed that during summertime the BVOC emissions exceed anthropogenic emissions in many countries, Simpson (1995) performed several simulations (one in which the isoprene emissions were turned off) and conclude that the isoprene emissions do not strongly influence the long-term average simulated O_3 concentrations. Using long-term measurements acquired at Ispra, Italy, Duane et al. (2002) however, showed that the contribution of locally emitted isoprene to the local ozone formation reached up to 50-75% during the summer of 2000. More recent studies that are mainly using two sets of simulations, one with and one without considering biogenic emissions, assessed the importance of BVOC on O_3 formation. Tagaris et al. (2014) showed that the European BVOC emissions increased the predicted MDA8 O_3 by 5.7% for July 2006. Jiang et al. (2019) have used two biogenic models, one predicting three times more isoprene emissions than the other, still the BVOC emissions contribute less than 10% of mean O_3 concentration in the summer of 2011. Churkina et al. (2017) indicate that biogenic emissions explain on average ~12% of modeled mean ozone in Berlin for two summers (June-August); yet, on hot summer days, these sources are responsible for up to 60% of the modeled MDA8 O_3 concentrations. Zhao et al. (2016) showed the use of a newer version of Model of Emissions of Gases and Aerosols from Nature (MEGAN) better reproduces the observed isoprene than the publicly available version of the MEGAN model integrated into WRF-Chem, which ultimately will impact the surface O_3 concentration. Moreover, Zhang et al. (2021) noted that the use of multiple versions of MEGAN has significantly influenced the ozone concentration due to the changes in simulated biogenic emissions.

One important sink for tropospheric ozone is given by ozone dry deposition, which is dominated by stomatal uptake by vegetation (Turnipseed et al., 2009, Lin et al., 2019, and references therein). Moreover, Lin et al. (2020) showed that a reduced ozone uptake by vegetation worsens the severe ozone pollution during heatwave events. When the water vapor pressure deficit is high, the plants close their stomata to prevent water loss. However, most models use the Wesely deposition scheme (Wesely, 1998) which does not account for humidity deficit and depends solely on temperature and radiation, and consequently, overpredicts the deposition of ozone under hot and dry conditions. Rydsaa et al. (2016) compared measurements of the stomatal conductance and stomatal ozone flux acquired during three summer field campaigns at three different sites in Italy with the modeled results predicted by using the Wesely scheme embedded within WRF-Chem. It has been shown that the model underestimated night-time stomatal ozone uptake, and consequently overpredicted ozone concentration in the stable night-time planetary boundary layer. The model also overestimated the daytime stomatal conductance, leading to underestimated midday ozone concentration, highlighting the existence of some systematic biases in the model parameterization.

In this study, we focus on the origin of elevated ozone levels observed over Germany during the 6 - 13 August 2015 and 1 - 8 August 2018 periods. The 2015 and 2018 summers have been the subject of several studies due to the severity in terms of temperature and precipitation. The summer of 2015 showed high drought conditions and was characterized by high temperatures in many parts of central and eastern Europe (Hoy et al., 2016, Ionita et al., 2016). Several heatwave episodes occurred from the end of June until September, which were linked to persistent blocking conditions and a northward deflection of Atlantic storm tracks (Ionita et al., 2016). Orth et al. (2016) showed that the 2015 summer was a concurrent dry and hot extreme in most of central Europe. Similarly, other

studies have analyzed the summer of 2018 in central Europe, which was characterized by extremely dry and hot conditions (Buras et al., 2020). Recently, Zscheischler and Fisher (2020) analyzed in more detail the compounding impacts of hot and dry events in Germany during 2018 (March-November). They showed that 2018 was record-breaking both in high temperatures and low precipitation.

The main goal of this study is to determine the contribution of different precursor emission sources to the modeled ozone concentration in Germany during these two periods. For this purpose, we perform a source attribution of tropospheric O_3 to both NO_x and volatile organic compound (VOC) precursors using the TOAST system (Tropospheric Ozone Attribution of Sources with Tagging) as described by Butler et al. (2018) and implemented in WRF-Chem as described by Lupaşcu and Butler (2019). Compared to previous studies, in which the impact of a certain emission source on total ozone concentration was simulated by switching on/off the emissions or using a source attribution of both NO_x and VOC based on the chemical regime, our tagging methodology allows us to investigate the separate contribution of the anthropogenic NO_x emitted in different European countries and regions of the world and the contribution of anthropogenic and biogenic VOC emitted in several regions to ozone levels seen in Germany during the aforementioned periods.

We first assess the model's ability to reproduce the hourly observed meteorological parameters and trace gas concentrations at all measurement stations in Germany. Then, using source attribution, we provide information about the contribution of different precursors to the total ozone concentration.

2 Model simulation

2.1. Regional model description and set-up

In this study, the WRF-Chem model version 3.9.1 (Grell et al., 2005, Fast et al., 2006) was used to simulate the high ozone concentrations observed in Germany during the 2015 and 2018 heatwaves. The analyzed periods are 6-13 August 2015 and 1-8 August 2018. For this purpose, we have set up two nested domains, using a 25-km, and 5-km grid spacing for a coarser domain that covers Europe, and an inner domain that encompasses Germany. The vertical coordinates use 38-sigma stretched levels extended up to 20 km a.g.l., with a ~50 m grid spacing adjacent to the surface and 11 levels located within 3 km of the ground.

The physics options used for this study include the Morrison double-moment microphysics scheme (Morrison et al., 2009), the Kain-Fritsch cumulus parameterization (Kain, 2004), the fast version of the Rapid Radiative Transfer Model (Iacono et al., 2008) for longwave and shortwave radiation. The surface and boundary layer schemes are the Noah-MP (Chen and Dudhia, 2001) and the Yonsei University PBL (YSU PBL) scheme (Hong, Noh, and Dudhia, 2006). Following the approach of Kuik et al. (2016), the CORINE dataset (EEA, 2014) was used instead of the default USGS land cover data set, as land use in Germany. In particular, the characterization of urban areas is better captured by the CORINE dataset (see Kuik et al. 2016, and Churkina et al., 2017).

Initial and boundary conditions for the meteorological parameters are taken from the ECMWF reanalysis (Era-Interim dataset). To limit the divergence of large-scale flow compared to the observed synoptic conditions, we have nudged the temperature and wind above the boundary layer for the outer domain. Biogenic trace gas emissions are calculated online using the MEGAN model (Guenther et al., 2006). Anthropogenic emissions (based on the year 2015) of CO, NO_x, SO_2, NMVOCs, PM10, PM2.5, and NH_3 are obtained from the TNO-MACC III emissions inventory (Kuenen et al., 2014) and used for both simulated years. Based on Mailler et al. (2013) work that investigated the impact of anthropogenic emission injection height in accurately simulating background SO_2,

NO$_2$, and O$_3$ concentrations, we applied the European vertical emissions profiles from the plume rise model of Bieser et al. (2011).

160 In this work, the extended tagged MOZART chemical mechanism described in Lupaşcu and Butler (2019) is used to track the ozone produced from NO$_x$ sources. We have also implemented within WRF-Chem a system that tracks ozone produced from VOC precursors, similar to Butler et al. (2018, 2020a). As in Lupaşcu and Butler (2019), the tagged O$_3$ species are advected independently, and to correct the numerical errors associated with the advection scheme, we use a mass fixer in which the sum of all combined tagged tracers is set equal to the corresponding
165 untagged concentration.

As in Butler et al. (2018, 2020a), two simulations are performed, one with NO$_x$ tagging, and another with VOC tagging using otherwise identical emissions. As the VOC tagged configuration is substantially more computationally expensive than the NO$_x$ tagged configuration, we employ a reduced set of tags in the VOC-tagged simulation. The full set of tags (as used in the NO$_x$ tagged simulation) is shown in Table 1. This set of tags enables
170 the simulated ozone in WRF-Chem to be attributed to emitted NO$_x$ from within and outside of Europe. Thirteen regions are defined for tagging emissions within the WRF-Chem domain, and another four regions are defined outside of the WRF-Chem domain, with tagged emissions and ozone from these regions transported into WRF-Chem via the lateral boundaries (see below). In addition to these geographical tags, which are applied to anthropogenic emissions, we define four "global" tags (not associated with emissions from any specific
175 geographical region) to track the ozone produced from biogenic and biomass burning emissions, lightning NOx, and stratospheric input.

For the VOC tagged simulations, we no longer need the "lightning" tag, but instead, we define an additional tag to account for methane as an ozone precursor. Instead of tagging anthropogenic VOC emissions with the full set of regions shown in Table 1, we use a reduced set of regions; the anthropogenic VOC emissions are tagged for
180 two regions: Europe (ANTE) and the rest of the world (ANTW). Instead of a single global tag for biogenic VOC emissions (as used in the NO$_x$ tagged simulation), we define four regional tags: Berlin (BIOB), the rest of Germany (BIOG), the rest of Europe (BIOE), and the rest of the world (BIOW). The number of explicitly tagged anthropogenic source regions is reduced in the VOC tagged simulation due to the higher computational requirements of the VOC tagging compared with NOx tagging (Butler et al., 2018, 2020a). Moreover, as noted by
185 Butler et al. (2018, 2020a) the contribution of anthropogenic VOC emissions to the total ozone during summer is reduced compared to the contribution of anthropogenic NOx emissions.

2.2. Chemical initial and boundary condition

As in Lupaşcu and Butler (2019), the boundary conditions for several HTAP2 source regions (Asia, North America, oceanic sources, and rest of the world), and natural types (biogenic, biomass burning, lightning
190 emissions, and stratospheric ozone) are obtained from the extended CAM-Chem version 1.2 simulations. For this purpose, we performed two model simulations using the extended NO$_x$ and VOC tagging mechanisms described in Butler et al. (2020a) for 2015 and 2018. The HTAP_v2.2 emission inventory (Janssens-Maenhout et al., 2015) was used to provide anthropogenic emissions. Biomass burning emissions for 2015 and 2018 are taken from the FINN inventory (Wiedinmyer et al., 2011). Biogenic emissions of NO$_x$ and VOC are prescribed (Tilmes et al.,
195 2015).

3 Observations

Observations of ozone, NO_2, and NOx are provided by the German Environment Agency UBA (Umweltbundesamt), which collects hourly surface pollutant observations from several hundred stations located across Germany, run by the Federal States. Also, the modeled 2 m temperature, mean sea level pressure, 10 m wind speed, and direction were compared with observations obtained from the German Weather Service (DWD) (Kaspar et al., 2013). For this purpose, we used the observed meteorological data retrieved from the DWD ftp site (ftp://ftp-cdc.dwd.de/pub/CDC/observations_germany/climate/hourly/). Additionally, we have used —2m-temperature from the reanalysis ERA5 (Herbach and Dee, 2016) that provides hourly data on a regular latitude-longitude 0.25°x0.25° spatial resolution as a proxy for observed daily maximum 2m-temperature (T2MAX) at the air quality station locations.

4 Results

4.1 Evaluation of the regional model

Due to the strong links between the meteorological parameters and ozone concentrations in the atmosphere (see Coates et al., 2016, Otero et al., 2016), we have assessed the ability of the WRF-Chem model to simulate the temperature, pressure, relative humidity, and wind speed and direction temporal variability over Germany. To do so, we evaluated the modeled meteorological fields against observations using statistical scores including mean bias, normalized mean bias (NMB), index of agreement (IOA), and the correlation factor between hourly simulated and measured values (r) (see Appendix 1).

Tables 2 and 3 show that the WRF-Chem model reproduces quite well the 2m temperature, surface pressure, and mean sea level pressure over Germany for both periods. On average, WRF-Chem overestimates observed surface pressure by less than 4.3 hPa and the mean sea level pressure by less than 0.8 hPa and reproduces very well the temporal evolution (r's > 0.92). The modeled 2m temperatures are on average close to those observed both in terms of predicted values (NMB's of -0.3%) and temporal evolutions (r > 0.84). At most of the observational sites, the model underestimated the nighttime 2m temperature is overestimated and the model underestimates the daytime temperature (Fig. 1). Therefore, the T2MAX is underestimated, on average, by 1.1° C in 2015 and 1.4° C in 2018, still lower than Wyszogrodzki et al. (2013), Chen et al. (2014), Karlický et al. (2020). The simulated relative humidity is fairly close to the observed one (NMB's of 14.5 and 20.1%, r's > 0.75). The relatively low NMB of wind direction suggests that the atmospheric flow is quite well reproduced. We note that the NMB of wind speed simulated by WRF-Chem is quite high (35.2% in 2015 and 31.6% in 2018). Previous work with the WRF-Chem model has also noted a high bias for simulated wind speed, especially when low wind speeds are observed (Fast et al., 2014, Gomez-Navarro, 2015, Solazzo et al., 2017, Kehler-Poljak et al., 2017, Gao et al., 2018). Tao et al. (2020) showed wind speeds' NMB of 54% at 5 km resolution as our setup. Gao et al. (2018) mentioned the errors in terrain data and reanalysis and relatively low horizontal and vertical resolution of the model among the factors contributing to overestimated wind speeds under calm wind conditions. Hence, we expect that horizontal mixing of ozone and emitted pollutants will be artificially enhanced in our simulations.

Tables 4 and 5 present the evaluation for the modeled trace gases at the "background" sites located in the inner domain for the 2015 and 2018 simulations. These "background" sites include "urban background", "suburban background" and "rural background". The model underestimates the observed concentrations and reproduces reasonably well the hour-to-hour variability of NO_2, and NO_x during both analyzed periods. Generally, the NO_2

and NO$_x$ concentrations are slightly overestimated at the "rural background" stations, and underestimated at "suburban and urban background" stations. This behavior has been also noted by Kushta et al. (2019) and Ghermandi et al. (2020). The underestimation of NO$_x$ at urban stations is mostly an effect of the spatially resolved traffic emission totals, while the overestimation at "rural" stations indicates that the NO$_x$ could be transported from the cities to the nearby rural areas. These discrepancies between modeled and observed NO$_x$ species could be related to 1) the errors associated with the predicted wind speed and direction which can lead to the displacement of modeled parcel of air relative to the observed values; 2) errors in the emissions inventory; 3) relatively low model resolution that could lead to underestimated emissions gradients as well as to increased diffusion of emission into grid cells and therefore the modeled grid cell concentration may not correctly represent the observed concentrations. Kuik et al. (2018) showed that during the interval 06:00-17:00 UTC the traffic NO$_x$ emissions could be underestimated by a factor of 3 in the urban area of Berlin, so we might assume this could be also the case for other German cities. Several other studies, such as Tuccella et al. (2012), Pirovano et al. (2012), Georgiu et al. (2018), have also noted the overall tendency of chemical transport models to underestimate the NO$_x$ concentrations at the European level.

The modeled O$_3$ concentration is quite well reproduced (NMB's of 2.3% and -0.9% in 2015 and 2018). The lower O$_3$ bias at "rural" stations compared to those seen at "suburban and urban background stations" could be a result of an increase in the NO titration effect due to NO$_x$ overestimation at rural stations. The comparison of hourly modeled and observed O$_3$ at each measurement station (see also Fig.1) reveals a persistent modeled overestimate of nighttime concentration and an underestimation of midday concentrations. The errors in predicting accurately the meteorological inputs such as nighttime boundary layer height could also be associated with the nighttime overprediction of surface ozone. Among the conditions that could lead to the underprediction of ozone peak value during the daytime, we could also point to the underestimation of T2MAX, uncertainties of emissions, both from anthropogenic (NO$_x$) and biogenic sources, as well as an overprediction in wind speeds that will transport further downwind the locally emitted precursors, which ultimately leads to a reduced local O$_3$ formation rate. During AQMEII-2 (Air Quality Model Evaluation International Initiative), the working groups using WRF-Chem reported an overall underestimation of the summer O$_3$ (Im et al., 2015). Tuccella et al. (2012) showed that, in August 2007, WRF-Chem tends to overestimate the low O$_3$ concentrations and underestimated those situated at the high end of the O$_3$ concentration distribution (see their Fig. 3).

The model is biased low when predicting surface MDA8 O$_3$ (NMB's of -3.3% and -9.7% in August 2015 and August 2018, respectively). The temporal and spatial variability are well reproduced during these two events (r> 0.74 and IOA >0.73). Since the MDA8 O$_3$ concentrations are influenced by ozone maxima values, the consistent underestimation of peak ozone values is also noted by several models (Tuccella et al., 2012, Im et al., 2015, Oikonomakis et al., 2018, Visser et al., 2019, Mertens et al., 2020). Visser et al. (2019) showed that, in July 2015, the European mean bias for MDA8 O$_3$ was -14.2 µg/m^3, while Oikonomakis et al. (2018) noted that the model consistently underestimates the afternoon (12:00-18:00 UTC) observed O$_3$ values above 50 ppb for the summer of 2010. Moreoever, Tuccella et al. (2012) noted an MB for MDA8 O$_3$ of -5 µg/m^3 in 2007. Kryza et al. (2020) showed an NMB for MDA8 O$_3$ of ~ -15% during the summers of 2017 and 2018.

In summary, the model simulated fairly well the diel and multiday variation of meteorological parameters and trace gases concentrations and slightly underestimates the peaks of temperature and ozone. Nevertheless, we acknowledge that a more comprehensive evaluation would also require the comparison between modeled and observed isoprene and its oxidation products. These chemical variables play a crucial role in increasing O$_3$ under

summer conditions, but unfortunately, they are not routinely measured. Expansion of routine air quality measurements to include biogenic VOCs or their oxidation products such as formaldehyde could significantly help with model evaluation.

4.2 Characteristics of modeled and observed surface concentration

In this section, we investigate the variability of O_3 concentration levels under two different O_3 peak events in Germany focusing on the 6 – 13 August 2015 and 1 – 8 August 2018 periods and provide a possible explanation on why, although the model captures well the mean O_3 concentrations, it fails in reproducing the observed O_3 peaks. Table 6 shows the percentage of stations where the daily MDA8 O_3 target value of 120 µg/m^3 was exceeded. Figures 2 and 3 depict the surface maps of daily observed and modeled MDA8 O_3 concentrations during the high ozone episodes. While the model captures the spatial and temporal observed pattern of MDAO$_3$, it usually underestimates the peak of MDA8 O_3 concentrations, as also shown in Table 6. This behavior is accentuated when the model fails to simulate the observed precipitations (not shown).

The synoptic situation during the analyzed periods is depicted in Fig. S1 and Fig. S2. Both years present similarities in their synoptic circulation patterns, although there are some small variations. In 2015, at the beginning of the period, the weather in Germany was influenced by a relatively high-pressure field situated in a saddle formed by a ridge of the Azores Anticyclone and an anticyclone centered over NE Scandinavia. The Azores' ridge, gradually extended towards the East, was transformed into a blocking ridge over central Europe. This blocking pattern has two stagnant low-pressure systems on the edge, one in the North Atlantic and the other over North-East Africa. At the same time, the vertical structure was influenced by a ridge that favors the intrusion of warm tropical air coming from Africa far to the north of Europe. These ridges formed a dome of high pressure that led to stagnant weather conditions characterized by low wind speed, strong insolation and subsidence, and high temperatures. Hence, the atmospheric subsidence associated with the anticyclonic field, leading to particularly stable atmospheric conditions, contributes to explaining the elevated ozone seen over southwest Germany in the first part of the period. As also shown in Otero et al. (2022), over Germany during the period 1999–2015, atmospheric blocking leads to temperature anomalies > 5 °C that induces MDA8 O_3 anomalies >20 µg/m^3. An occluded front on August 9, 2015, led to reduced ozone values in West Germany, and it was followed by a warm front that affected North Germany, which explains the low ozone values observed/modeled in this region. In 2018, the observed ridge of the Azores High has gradually increased in magnitude and it became centered over the middle of the Atlantic. This high-pressure field has slowly retreated towards the West, thus the surface pressure influencing Germany became shallow and favored the appearance of a cold frontal system and its moderate winds and cloudy/rainy weather that prevailed on 5 – 6 August 2018.

Using the scatter plots depicted in Fig. 4, we compare our modeled MDA8 O_3 and the daily T2MAX pair against the observed MDA8 O_3 and ERA5 T2MAX pair. We choose ERA5 T2MAX as a proxy for observed T2MAX since these measurements are not available at air quality station locations. We note that the modeled T2MAX and MDA8 O_3 are relatively low correlated (r's of ~ 0.45); for both periods, the slopes of the linear fit to modeled MDA8 O_3 and T2MAX are comparable (3.24 µg m^{-3}/°C and 4.04 µg m^{-3}/°C). When the same analysis is applied to the observed MDA8 O_3 concentrations and ERA5 temperatures pair, we remark a relatively high correlation of these variables (r=0.76 and 0.62), a high ozone–temperature slope (5.6 and 5.2 µg m^{-3}/°C) compared to the modeled ozone–temperature slope. As previously noted, the model failure in reproducing the meteorological variables is not conducive to O_3 formation, and this could explain the model's inability to capture the observed MDA8 O_3

sensitivity to T2MAX. Clearly, the underestimation of T2MAX cannot be the only factor contributing to the differences in the modeled and observed MDA8 O_3-T2MAX slopes and intercept values, as +30 µg/m³ biases occur at T2MAX lower than 20° C. A scatter plot of modeled vs observed MDA8 O_3 and T2MAX (see Fig. S3) shows that, generally, the T2MAX is underestimated. While the observed values of MDA8 O_3 reach more than 120 µg/m³, the corresponding model values tend to be underestimated; for observed values below 75 µg/m³, the modeled values are generally overestimated. Pusede et al. (2015) haves also shown that other meteorological factors, including the advection and vertical mixing, have an indirect impact on chemistry, hence on ozone production.

Otero et al (2016) showed that in summer, apart from the temperature that is the main driver that dominates high ozone levels, relative humidity plays a negative effect on ozone levels. Hence, the high modeled relative humidity (see Tables 2 and 3) together with overestimated shallow precipitation (see Figures S4 and S5) suggests a reduction in ozone production due to enhanced cloudiness. As noted in Section 4.1, the overestimation of simulated wind speed could enhance the horizontal mixing of ozone and emitted pollutants in our simulations. It is well known that the ground-level ozone depends, amongst other factors, on the level of ozone precursors, such as biogenic VOCs, especially isoprene, and anthropogenic NO_x. Unfortunately, the isoprene concentrations, one of the main VOC precursors of ozone that reacts by the high-NO_x pathway to produce ozone, are not monitored at the German network sites, so we can't assess the model's ability to reproduce this pollutant. Fast et al. (2014), using the measurements collected in May – June 2010 during the Carbonaceous Aerosol and Radiative Effects Study (CARES) and the California Nexus of Air Quality and Climate Experiment (CalNex), showed that even if the model reproduces the temporal isoprene variation, still, daytime mixing ratios of isoprene are usually a factor of 2 too low. Moreover, the underestimation of the modeled surface temperature could lead to an underestimation of isoprene emissions. Guenther et al. (2012) showed that changes in meteorology could lead to a change of ~15% in isoprene and terpene emission fluxes. Thus, the lack of isoprene and the underestimation of predicted NO_x (see Tables 4 and 5) could also explain the underestimation of MDA8 O_3.

The accurate prediction of surface ozone concentration remains a challenge because the concentration depends not only on emissions but also on a detailed representation of physical and chemical processes. Rydsaa et al (2016) showed that WRF-Chem underestimates the modeled nighttime stomatal ozone uptake that leads to too high modeled estimates of ozone concentration in the stable nighttime planetary boundary layer. Also, they showed that during daytime the modeled stomatal conductance is higher than the observations, and thus too low midday modeled ozone concentration. This is also consistent with our simulations (see Fig. 1). As in Rydsaa et al. (2016), our Fig. 1 shows a low midday modeled ozone concentration when compared with observation, and high modeled night-time ozone. The stomatal resistance in the Wesely scheme is calculated using the first layer (surface) temperature and solar radiation. Thus, the lasting high 2m temperature in 2018 (maximum of 34.3° C, and median of 21.8° C) compared to those modeled in 2015 (maximum of 36.1° C, and median of 19.6° C) leads to high stomatal resistance, consequently a reduced ozone uptake from vegetation that ultimately leads to an increased modeled surface concentration. Turnipseed et al. (2009) also showed that a major sink for ozone in the canopy is the direct uptake by vegetation through the stomata. Jiang et al. (2018) showed that a reduction of stomatal conductance leads to an increase in leaf temperature, and consequently more isoprene emissions from plants. Using a global model, Gong et al. (2020) found that O_3-induced inhibition of stomatal conductance can increase surface O_3 by 1.0-1.3 ppbv in western Europe. Visser et al. (2021) also showed that daytime stomatal conductance is overestimated. As noted in Section 4.1, several studies showed a systematic underestimation of WRF-Chem's peak

O$_3$ values (Visser et al., 2019, Oikonomakis et al., 2018, Tuccella et al., 2012, Kryza et al., 2020). Stanier et al. (2021) noted that high MDA8 O$_3$ values were biased low as in our Fig. 4, while Lu et al. (2021) noted the MDA8 O$_3$ was in general underestimated in July 2018.

Moreover, as a potential effect of climate change, the high extreme temperatures in the future will hinder the O$_3$ control, thus knowing which sources of emissions are contributing to the severe O$_3$ pollution episodes will help to design effective emissions control.

4.3 Influence of different emission sources on hourly ozone at individual stations

In the following, we examine the impacts on O$_3$ concentrations in Germany of NO$_x$ and VOC precursors for 14 individual background stations, which are representative of the geographical distribution over the German states (see Table 7). Figures 5 and S6 summarize the mean absolute and relative contribution of NOx and VOC precursors to hourly surface O$_3$ for the analyzed periods. We note that when we attribute O$_3$ to NO$_x$, the southern stations (Baden-Württemberg, Hesse, Rhineland-Palatinate, and Saarland) show a large contribution from the German source region (up to 35.2 µg/m^3 (34.4%) in 2015 and 33.4 µg/m^3 (34.7%) in 2018), while for the remaining station the German NO$_x$ emissions were not seen as a dominant source, Central Europe being one of the most important contributors to the total ozone (up to 30.4 µg/m^3 (29.1%) in 2015 and 19.7 µg/m^3 (22%) in 2018). When we attribute O$_3$ to VOC, we note that CH$_4$ is the most significant contributor to the total O$_3$ (up to 31.21 µg/m^3 (36.3%) in 2015 and 31.5 µg/m^3 (37.2%) in 2018), followed by German and European BVOCs emissions. Further, we will analyze the hourly variation in O$_3$ concentration to examine the impact of variation in anthropogenic and biogenic emissions, meteorology and long-range transport. Figures 6 5 and 7 6 show the contribution of NO$_x$ precursors to hourly surface ozone in 2015 and 2018, while Figures 8 7 and 9 8 show the contribution of VOC precursors during these periods.

The stratospheric contribution is similar in both simulations. Considering that the stratospheric ozone is advected within the domain through the lateral boundaries, the small differences in the stratospheric contribution noticed between the NO$_x$- and VOC-tagged simulations are related to the difference coming from CAM-Chem as explained by Butler et al. (2018). The attribution of O$_3$ to different sources helps to identify the ozone from stratosphere-troposphere exchange. For both analyzed events, the variability revealed periods in which stratospheric ozone contribution can reach 70 µg/m^3 (53%). As an example, the intrusion of stratospheric ozone seen at the beginning of August 2018 in north Germany can be associated with the Icelandic low that reaches its minimum pressure and geopotential height on July 30, 2018, which led to a strong downward wind component, therefore an increase of stratospheric ozone transported to the surface (see Fig. S2). As shown in Lupaşcu and Butler (2019), the surface stratospheric O$_3$ is attributed to the transport of stratospheric O$_3$ concentrations that originates from the lateral boundary concentrations (taken from the CAM-Chem extended model). Clockwise winds at the edge of the Azores High brought air pollutants such as stratospheric ozone and its precursors from Iceland and North-Atlantic to north Germany. The blocking situation impedes the westerly winds, therefore the transport of stratospheric ozone decreased. Kalabokas et al. (2013) showed that summer ozone maxima in Cyprus are observed when rich-ozone air masses subside from the upper troposphere, and consequently, they transport stratospheric O$_3$. Similarly, our study shows that the stratospheric ozone may also have a large influence when the MDA8 O$_3$ peak values are observed for the northern regions of Germany. Yet, the prevailing southerly winds modeled in south Germany blocks the transport of stratospheric ozone in these regions. Future work should examine the stratospheric O$_3$ intrusions and their impact on tropospheric O$_3$ ozone production.

4.3.1 Attribution of ozone to NOx emissions

400   Figures $\underline{6}\sout{5}$ and $\underline{7}\sout{6}$ show the German and remote contribution of NO_x emissions to hourly O_3 at individual stations in different German states, as well as the observed O_3 concentrations and modeled wind speed and direction. The time series of observed O_3 concentrations were well captured by the model, although it fails in reproducing the high-end of observed O_3 values, as noted above. It can also be seen that the contribution of different NO_x source regions and source types to the ozone time series at each station varies greatly over time and space. The average

405   contributions of the global HTAP2 regions associated with long-range transport were ~20% to the total O_3 and remained relatively stable in both years. Emissions from lightning and biogenic NOx have the least contributions to total O_3 during these episodes.

For both episodes, the contribution of German NO_x ~~German~~ emissions to the ozone concentration is small most of the time in the northern states (from 6.7 µg/m^3 (6 %) in 2015 and 7.6 µg/m^3 (8.3%) in 2018 in Mecklenburg-

410   Vorpommern to 9.0 µg/m^3 (16%) in 2015 and 12.5 µg/m^3 (13.1%) in 2018 in Brandenburg), whereas the peak ozone events in the south-western and western German stations are mainly driven by German NO_x sources (up to 35.31 µg/m^3 (33.6%) in 2015 and 33.5 µg/m^3 (33.4 %) in Baden-Württemberg), usually exceeding the total contribution of surrounding source regions. The peak ozone events in the southern states are also generally higher than the peak ozone events in the northern states. At the analyzed stations, a significant positive correlation

415   between ozone from local NO_x sources and total ozone is found in both years (r's of 0.57 in Bavaria to 0.89 in Thuringia in 2015 and 0.33 in Mecklenburg-Vorpommern to 0.84 in Saxony-Anhalt in 2018). This emphasized the importance of NO_x German sources as a key factor that drives high levels of O_3. These results further revealed that the high contribution of NO_x German sources to hourly O_3 is strongly connected with low wind speed values, endorsing the impact of high-pressure systems on serious local O_3 pollution. Furthermore, we note that high wind

420   speeds bring O_3 pollut~~ed air~~ from regions upwind of our stations' location.

The main NO_x contributors to stations differ when we compare the O_3 pollution episodes in 2015 with those in 2018. As can be seen in Figs. $\underline{6}\sout{5}$ and $\underline{7}\sout{6}$, in 2015, the stations in Lower Saxony, North Rhine-Westphalia, Rhineland-Palatinate, Hesse, and Saarland are influenced by transport from sources in Benelux (up to 30 µg/m^3, 31.7%), France (up to 63 µg/m^3, 48.6%), and Italy-Switzerland (up to 22 µg/m^3, 14.8%) at the beginning of the

425   analyzed period, while in 2018 the same source regions have a significant contribution to the same stations at the end of the analyzed period, up to 41 µg/m^3 (28.9%), 57 µg/m^3 (42.9%) and 29 µg/m^3 (33.7%) µg/m^3, respectively. The prevailing winds that favor the influence of these source regions are from the southwest. If the dominant wind direction is from the south, the German sources can explain more than 50% of total O_3. Among stations in north Germany (Schleswig-Holstein, Mecklenburg-Vorpommern, Berlin, Brandenburg) we note a sporadic contribution

430   from the Scandinavian Peninsula (SCA) and Baltic and North Seas (BNS) in both years.

The outflow of ozone from other European regions plays a significant role in ozone pollution episodes, as the wind direction shifts from one day to another. Central Europe (CEN) is responsible for a remarkably constant share of ~25 % (ranging from 19 to 30 µg/m^3) of the total ozone in 2015 at stations in Berlin, Brandenburg, Saxony-Anhalt, Thuringia, Saxony, and Bavaria, while in 2018 it exhibits an erratic contribution to the total O_3 concentration (see

435   Figs. $\underline{6}\sout{5}$ and $\underline{7}\sout{6}$). Among stations within Baden-Württemberg, Bavaria, and Saxony, we distinguish a noticeable influence from the~~of~~ rest of the world (up to 32 µg/m^3, 23%), and RBT (Russia, Belarus, Ukraine, Turkey, Azerbaijan, Armenia, and Georgia) (up to 15 µg/m^3, 13.8%) in 2018, and of SEE (Bulgaria, Romania, Moldavia, Albania, Slovenia, Croatia, Serbia, Montenegro, Macedonia, Greece, and Cyprus) (up to 10 µg/m^3, 11%) in 2015. The large contribution of German and European sources during these events indicates that a reduction of high O_3

440 pollution could not be achieved without a regional collaboration of controlling emissions sources within Europe. However, we note that the transport of ozone and its precursors could be exacerbated since our model does not capture the stagnant conditions and overestimates the wind speeds observed in calm wind conditions by more than 60% in both years.

Even though we identified the main source regions that could explain the origin of O_3 in different regions of
445 Germany when the NO_x-tagged mechanism is employed, we note that there is a large variability within the same region. For example, in 2018, in Brandenburg, the contribution of the stratospheric ozone is higher in the northern area of this region in comparison with the southern area (see Fig. S74). In Baden-Württemberg (Fig. S74), the stations located in the east of the region are largely influenced by CEN (Central Europe), while those located westward exhibit the largest contribution from German sources and FRA (France).

450 Moreover, the simulations accounting for two pollution episodes occurring in two different years show that changes in circulation patterns between those two years can affect the contribution of different NO_X emission sources to total O_3. Mitigation measures targeting anthropogenic NOx emissions for the reduction of ambient ozone should focus on widespread regional reductions rather than targeted local reductions.

Shipping activities in the Baltic and North Seas have also contributed to the hourly O_3 (see Figs. 65, 76). This is
455 consistent with previous work (i.e., Lupaşcu and Butler, 2019, Pay et al., 2019, Aksoyoglu et al., 2016, Jonson et al., 2020) that highlighted the impact of shipping on ozone production near coastal regions. Apart from reinforcing the role of shipping on ozone predicted in coastal areas, our ozone attribution also shows that the inland regions, such as Bavaria and Baden-Württemberg are also impacted by ozone produced from ship's emissions (up to 3.7 µg/m^3 (3.8%) and 4.7 µg/m^3 (5.2%), respectively, in 2015 and 7.2 µg/m^3 (6.6%) and 9 µg/m^3 (9.8%) in 2018).
460 This underlines the effect of transport of O_3 produced from possibly remote NO_x emissions on total O_3 for mitigation purposes.

4.3.2 Attribution of ozone to VOC emissions

At the same stations, we investigate the impacts on O_3 concentrations in Germany of VOC precursors (see Figures 87 and 98). As in Butler et al. (2020a), methane oxidation is one of the main contributors to the total ozone and it
465 has an almost constant contribution throughout the analyzed periods, ranging from 23.3±5.8 µg/m^3 (22.7±2.3%) to 31.2±5.5 µg/m^3 (36.4±5.9%) in 2015 and from 25.6±6.4 µg/m^3 (33.7±7.3%) to 31.4±8.4 µg/m^3 (38.3±9%) in 2018. Most of the ozone from CH_4 as well as CH_4 itself is coming from the lateral boundaries. Even though we consider the domain-wide methane emissions in our system, we expect as in Butler et al. (2020b) that the highest share of ozone coming from methane to be attributed to intercontinental transport. European anthropogenic VOC
470 sources contribute only modestly to the O3 concentration, with an average contribution of 9.3±5 µg/m^3 (10±3.6%) in 2015 and 7.9±4.7 µg/m^3 (8.6±3.9%) in 2018. Apart from the stratospheric intrusion event in 2018, most of the spatial and temporal variability in peak ozone is driven by the production of ozone from biogenic VOC emissions. The ozone attributed to biogenic VOC emissions also exhibits a geographical pattern, as for the NO_x-tagged simulations. The highest share of ozone from biogenic sources is modeled in the south and south-west of Germany,
475 where peak ozone is also generally higher, as noted for NO_x source attribution. This region is mostly covered by broadleaf deciduous trees (EEA, 2006), a vegetation class that has especially high isoprene emissions (Guenther et al., 2006, Pfister et al., 2008). The high temperatures and the large coverage of biogenic-emitting species in the afore-mentioned areas can explain the high levels of ozone in these regions. The contribution of biogenic VOCs to total O_3 is higher during the day, reflecting the onset of biogenic VOC emissions that combined with the high

480   temperatures promotes the photochemical production of O_3 from NO_x and VOC precursors. Comparison of high ozone events in Figs. 65 and 76 with the corresponding events in Figs. 87 and 98 (see also Figs S8 and S9) show that biogenic VOC contribute to O_3 when they react with anthropogenic NO_x from nearby sources.

As for NO_x-tagging, the ozone coming from German biogenic emissions correlates relatively well with the total ozone in both years (r's of 0.68 in Mecklenburg-Vorpommern to 0.88 in Lower Saxony in 2015 and 0.43 in

485   Mecklenburg-Vorpommern to 0.80 in Hesse in 2018). Similar to NO_x source attribution, we note that the outflow of ozone coming from biogenic sources from the rest of Europe has a considerable impact on ozone concentration seen at these stations. Moreover, at the analyzed stations, the ozone coming from biogenic sources outside Germany also displays a good correlation with the total ozone (r's of 0.48 in Mecklenburg-Vorpommern to 0.75 in North Rhine-Westphalia in 2015 and 0.15 in Saarland to 0.62 in 2018 in Thuringia). The low correlation between

490   ozone coming from the German NO_x or VOC precursors and total ozone noticed mostly in Mecklenburg-Vorpommern is related to a low predicted photochemistry, as also indicated by T2MAX values (not shown).

The average contribution of ozone coming from German biogenic emissions ranges from 4.65% (4.1 µg/m^3) for Mecklenburg-Vorpommern to 25.3% (26.1 µg/m^3) for Baden-Württemberg in 2015 and from 5.6% (4.84 µg/m^3) for Mecklenburg-Vorpommern to 24% (23.2 µg/m^3) for Baden-Württemberg in 2018, within the range of averaged

495   contribution shown by Mertens et al. (2020). Mertens et al. (2020) used a source attribution method that attributes O_3 to all precursors, without distinguishing between NO_x and VOC. They showed that during extreme ozone events the contribution of the land transport sector is gaining importance, and, more, the contribution of the biogenic emissions to ozone levels is increasing during these events. Their work indicates that 18.8±0.3% of their modeled O_3 for the June-August 2008-2010 period could be explained by the large contribution of biogenic emissions

500   (consisting of both biogenic VOC and soil NO_x). In contrast, our approach can separate the influence of these two distinct sources. At the analyzed stations we find that, on average, the soil NO_x emissions explain just 7% of modeled O_3, while 37% of modeled O_3 is attributed to all European BVOC emissions, with 14% of ozone due to BVOC emissions just from Germany. These findings suggest that the biogenic emissions that contribute to the high ozone levels seen in Mertens et al. (2020) are mainly attributed to the BVOCs, and not to the soil NO_x. Our

505   focus on peak ozone episodes favors the enhancement of biogenic emissions, consequently of predicted O_3 attributed to those sources. Furthermore, Pay et al. (2019) used an O_3 source apportionment method that used all precursors in a single run and utilized the H_2O_2/HNO_3 ratio to determine if O_3 is VOC- or NOx-sensitive. They showed that their source sector which includes biogenic emissions could explain up to 8% of daily mean modeled O_3 during days when the O_3 target values of 120 µg/m^3 are exceeded in Spain. The relatively low contribution of

510   biogenic sources to daily mean O_3 suggests that their region of interest was mostly in a NO_x-limited regime throughout the simulation. Moreover, their study highlighted the need of attributing the BVOCs to an individual source since these emissions represent 70% of VOC emissions in Spain. Our source attribution method allows us to investigate the contributions of these specific emission sources to ozone, and, in addition, we can separate contributions from biogenic emissions of NO_x or VOC precursors on ozone levels. Our method also allows a direct

515   quantification of O_3 coming from BVOC in comparison with other studies in which the emissions of biogenic were simply turned on and off (i.e., Lee et al., 2014, Churkina et al., 2017, Sun et al., 2021).

Figure 109 shows the relative contribution of BVOC and its precursors from Germany and the rest of Europe to ozone peak events in the hotspot area of Baden-Württemberg where the average predicted ozone concentration is 115 and 102 µg/m^3 in 2015 and 2018, respectively. These results are averaged over each grid cell defined as Baden-

520   Württemberg. The average contribution of ozone from German biogenic emissions is higher than 20 µg/m^3 (~23

%) in both years (see Fig. 10). We note that the temporal variation of total O_3 and O_3 coming from German BVOC emissions are in good agreement (r's of 0.72 and 0.65). The German isoprene concentrations predicted in Baden-Württemberg build-up in the early morning and evening and are low during the daytime due to the reaction with OH that ultimately leads to ozone formation in the area. Moreover, the ratio BVOC/NO_x is higher during daytime (not shown) and it favors the production of O_3 by NO_x, leading to an enhanced O_3 formation from German and other European biogenic sources. On the other hand, Figure 10 also portrays that the diurnal variation in the ozone coming from German biogenic sources is not dominated by the diurnal variation in biogenic isoprene emissions and the peaks of ozone from biogenic sources are disconnected from local emission peaks. These findings suggest that the formation of O_3 from isoprene oxidation takes place either in the vicinity of the source or occurs in the regions downwind of Baden-Württemberg. Hence, the Baden-Württemberg biogenic VOC emissions are not the sole factor that influences the ozone formation and other meteorological and chemical processes affect the diel variation of ozone having a biogenic origin. Furthermore, Fig. 10 depicts a relatively stable contribution of ozone coming from biogenic sources originating outside Germany (on average 18.6 $\mu g/m^3$ (16.4±3.7%) and 13.8 $\mu g/m^3$ (13.3±8.7%) in 2015 and 2018, respectively) to the baseline ozone, a consequence of the long ozone lifetime and the horizontal transport of ozone to Baden-Württemberg. Given the uncertainties in biogenic emissions estimates (Zhao et al., 2016, Zhang et al., 2021), a future study should include the use of MEGAN v2.1 as described by Zhao et al. (2016).

5   Conclusions

The WRF-Chem model was used to perform a source attribution of German surface ozone from emitted NO_x and VOC during two peak ozone events that took place in 2015 and 2018. The results from our simulations demonstrate that the peak ozone concentrations, which are reached during episodes of high temperatures, can be primarily attributed to nearby emissions of anthropogenic NOx (from Germany and immediately neighboring countries) and biogenic VOC. Outside of these high ozone episodes, baseline ozone concentrations are attributed primarily to long-range transport, with ozone due to remote anthropogenic NOx emissions and methane oxidation adding to the tropospheric ozone background. Anthropogenic NMVOC emissions do not contribute significantly to peak ozone events, but rather make a modest contribution to the baseline ozone.

The attribution of modeled O_3 to NO_x emissions at 14 stations in Germany showed that depending on the geographical location of stations, the nearby sources could have a significant contribution to ozone formation (mostly in south Germany), whereas in north Germany the high ozone concentrations are associated with enhancement of transported ozone or brought from aloft. Westerly stations are more prone to be also influenced by ozone transported from France and Benelux, while easterly stations show a constant share of O_3 transported from Central Europe, more pronounced in 2015, highlighting the importance of prevailing winds on ozone pollution levels at a given location. When attributing modeled O_3 to VOC emissions we find that the German biogenic emissions account for the largest fraction of ozone during these episodes, and they exhibit the same geographical pattern, as for NO_x source attribution, stressing that the production of ozone depends on the local interplay among NO_x and VOC precursors. Our study also highlights the good correlation between ozone coming from German biogenic emissions and total ozone, although the diurnal variation in the ozone coming from biogenic sources is not dominated by the diurnal variation in biogenic emissions, and the peaks of ozone from biogenic sources are disconnected from local emission peaks. This suggests that the formation of O_3 from local German

560   biogenic VOC emissions is not the sole factor that influences the ozone formation and other meteorological and chemical processes affect the diel variation of ozone having a biogenic origin. Moreover, the relatively stable contribution of ozone coming from biogenic sources originating outside Germany to the baseline ozone underscores the combination of long lifetime and horizontal transport of ozone.

Shipping activities in the Baltic and North Seas have a great impact on ozone predicted in coastal areas, yet a small

565   amount of ozone from these sources can also be seen far inland, stressing the importance of transported ozone on pollution levels. These findings complement those of previous studies, such as Erikson et al., 2021, and references therein, that showed that regional actions are needed to reduce the peak ozone concentration during high ozone episodes. We have also shown that changes in circulation patterns between different peak O_3 episodes observed in 2015 and 2018 can affect the contribution of different NO_X emission sources to total O_3, as such same source

570   regions significantly impact the O_3 concentration at a given location at the beginning of the analyzed period in 2015 and the end of the analyzed period in 2018. Thus, the possible influence of multiple upwind source regions should be accounted for when mitigation strategies are designed.

Overall, this study provides useful findings on how emissions from local and remote sources influence the predicted O_3 and MDA8 O_3 during two high ozone episodes. Biogenic VOC emissions as well as the NOx emitted

575   in nearby regions enhance the O_3 production during episodes of higher temperatures. Given the high importance of biogenic VOC in determining the peak ozone concentrations, the lack of VOC measurements for evaluation of the modeled VOCs is another source of uncertainty in modeled ozone production. Previous studies highlighted that the model strongly underestimates the isoprene concentrations leading to an underestimation of the total ozone concentration, which might be the case for our study. It is noteworthy that, apart from modeled BVOCs, other

580   factors such as anthropogenic emissions can influence the oxidation mechanism of the BVOC used in our simulation. Thus, the use of a highly resolved emissions inventory and Aadditional VOC measurements, including biogenic VOC are necessary to improve our understanding of how well the modeled ozone precursors are simulated, consequently, the total O_3 concentrations.

Code and data availability.

585   The WRF-Chem model is publicly available on http://www2.mmm.ucar.edu/wrf/users/download/get_source.html. The modification introduced and described in Section 2 as well as the model data can be provided upon request to the corresponding author.

Appendix 1. Statistical scores

The main statistical metrics employed in this study are Pearson correlation coefficient (r), Mean Bias (MB),

590   Normalized Mean Bias (NMB), and Index of Agreement (IOA). These statistical indicators are defined as follows, with n the number of model–observation pairs, M the modeled values (with $\bar{M} = \frac{\sum_{i=1}^{n} M_i}{n}$ the averaged modeled value) and O the observations (with $\bar{O} = \frac{\sum_{i=1}^{n} O_i}{n}$ the averaged observed value):

$$MB = \frac{1}{n} \sum_{i=1}^{n} (M_i - O_i)$$

$$NMB = \frac{\sum_{i=1}^{n} (M_i - O_i)}{\sum_{i=1}^{n} O_i}$$

$$r = \frac{\sum_{i=1}^{n}(M_i - \bar{M})(O_i - \bar{O})}{\sqrt{\sum_{i=1}^{n}(M_i - \bar{M})^2}\sqrt{\sum_{i=1}^{n}(O_i - \bar{O})^2}}$$

$$IOA = 1 - \frac{n * \sqrt{\frac{1}{n}\sum_{i=1}^{n}(M_i - 0_i)^2}}{\sum_{i=1}^{n}((|M_i - \bar{M}| + |O_i - \overline{O}|)^2}$$

Author contributions

AL and TB designed the research. AL performed the model runs. The analysis of model runs was performed by AL with input from each co-author. AL drafted the paper with contributions from all the co-authors.

Acknowledgments

We acknowledge the use of the WRF-Chem preprocessor tools (bio_emiss, fire_emiss, mozbc) provided by the Atmospheric Chemistry Observations and Modeling Lab (ACOM) of NCAR.

Financial support

This work was hosted by IASS Potsdam, with financial support provided by the Federal Ministry of Education and Research of Germany (FBMBF) and the Ministry for Science, Research and Culture of the state of Brandenburg (MWFK).

References

Aksoyoglu, S., Baltensperger, U., and Prévôt, A. S. H.: Contribution of ship emissions to the concentration and deposition of air pollutants in Europe, Atmos. Chem. Phys., 16, 1895–1906, https://doi.org/10.5194/acp-16-1895-2016, 2016.

Analitis A, Michelozzi P, D'Ippoliti D, De'Donato F, Menne B, Matthies F, Atkinson RW, Iñiguez C, Basagaña X, Schneider A, Lefranc A, Paldy A, Bisanti L, and Katsouyanni K.: Effects of heat waves on mortality: effect modification and confounding by air pollutants. Epidemiology, Jan; 25(1):15-22. doi: 10.1097/EDE.0b013e31828ac01b, 2014.

Buras, A., Rammig, A., and Zang, C. S.: Quantifying impacts of the 2018 drought on European ecosystems in comparison to 2003, Biogeosciences, 17, 1655–1672, https://doi.org/10.5194/bg-17-1655-2020, 2020.

Bieser, J., Aulinger, A., Matthias, V., Quante, M., and Denier van der Gon, H. A. C.: Vertical emission profiles for Europe based on plume rise calculations. Environmental Pollution, 159, 2935–2946. https://doi.org/10.1016/j.envpol.2011.04.030, 2011.

Butler, T., Lupascu, A., and Nalam, A.: Attribution of ground-level ozone to anthropogenic and natural sources of nitrogen oxides and reactive carbon in a global chemical transport model, Atmos. Chem. Phys., 20, 10707–10731, https://doi.org/10.5194/acp-20-10707-2020, 2020a.

Butler, T. M., Leitao, J., and Lupascu, A.: Consideration of methane emissions in the modelling of ozone concentrations in chemical transport models. Final report, (Texte / Umweltbundesamt ; 67/2020), Dessau-Roßlau : Umweltbundesamt, 40 p., 2020b.

Butler, T., Lupascu, A., Coates, J., and Zhu, S.: TOAST 1.0: Tropospheric Ozone Attribution of Sources with Tagging for CESM 1.2.2, Geosci. Model Dev., 11, 2825–2840, https://doi.org/10.5194/gmd-11-2825-2018, 2018.

Chen, F. and Dudhia, J.: Coupling an advanced land surface-hydrology model with the Penn State-NCAR MM5 modeling system. Part I: Model implementation and sensitivity, Mon.Weather Rev., 129, 569–585, 2001.

Churkina, G., Kuik, F., Bonn, B., Lauer, A., Grote, R., Tomiak, K., andButler, T.M.: Effect of VOC Emissions from Vegetation on Air Quality in Berlin during a Heatwave Environ. Sci. Technol., 51, 6120-6130, doi: 10.1021/acs.est.6b06514, 2017.

Coates, J., Mar, K. A., Ojha, N., and Butler, T. M.: The influence of temperature on ozone production under varying NO_x conditions – a modelling study, Atmos. Chem. Phys., 16, 11601–11615, https://doi.org/10.5194/acp-16-11601-2016, 2016.

Chen, F., Liu, C., Dudhia, J., and Chen, M.: A sensitivity study of high-resolution regional climate simulations to three land surface models over the western United States. *Journal Of Geophysical Research-Atmospheres*, *119*, 7271-7291. doi:10.1002/2014JD021827, 2014.

Curci, G., Beekmann, M., Vautard, R., Smiatek, G., Steinbrecher, R., Theloke, J., and Friedrich, R.: Modelling study of the impact of isoprene and terpene biogenic emissions on European ozone levels, Atmos. Environ., 43, 1444–1455, https://doi.org/10.1016/j.atmosenv.2008.02.070, 2009.

Degraeuwe, B., Thunis, P., Clappier, A., Weiss, M., Lefebvre,W., Janssen, S., and Vranckx, S.: Impact of passenger carNOxemissions on urban NO2pollution – Scenario analy-sis for 8 European cities, Atmos. Environ., 171, 330–337,https://doi.org/10.1016/j.atmosenv.2017.10.040, 2017.

Duane, M., Poma, B., Rembges, D., Astorga, C., and Larsen, B.R.: Isoprene and its degradation products as strong ozone precursors in Insubria, Northern Italy, Atmos. Environ., 36 (2002), pp. 3867-3879, https://doi.org/10.1016/S1352-2310(02)00359-X.

EEA, 2014: CORINE land cover data 2006, updated, http://www.eea.europa.eu/data-and-maps/data/corine-land-cover-2006-raster-3, European 20 Environment Agency, Copenhagen, Denmark, 2014.

EEA (2006) European forest types. Categories and types for sustainable forest management and reporting. European Environment Agency, EEA Technical report No. 9/2006. ISSN 1725-2237 Available at: http://www.foresteurope.org/docs/other_meetings/2006/wfc/WFC_4_eea_technical_report_92006.pdf. Accessed 23 November 2020., 2006

Emmons, L. K., Walters, S., Hess, P. G., Lamarque, J.-F., Pfister, G. G., Fillmore, D., Granier, C., Guenther, A., Kinnison, D., Laepple, T., Orlando, J., Tie, X., Tyndall, G., Wiedinmyer, C., Baughcum, S. L., and Kloster, S.: Description and evaluation of the Model for Ozone and Related chemical Tracers, version 4 (MOZART-4), Geoscientific Model Development, 3, 43–67, doi:10.5194/gmd-3-43-2010, http://www.geosci-model-dev.net/3/43/2010/, 2010.

EU directive 2008/50/EC of the European parliament and of the council on Ambient Air Quality and Cleaner Air for Europe (http://eur-kex.europa.eu/LexUriServ/LexUriServ.do?uri=OJ:L:2008:152:0001:0044:en:PDF, last accessed April 6, 2018), 21 May 2008.

Fast, J.D., Gustafson, Jr, W.I., Easter, Jr, R.C., Zaveri, R.A., Barnard, J.C., Chapman, E.G., Grell, G., and Peckham, S.E.: Evolution of Ozone, Particulates, and Aerosol Direct Radiative Forcing in the Vicinity of Houston

665   Using a Fully Coupled Meteorology-Chemistry-Aerosol Model, J. Geophys. R. D. (Atmospheres) 111 (D21): D21305. doi:10.1029/2005JD006721, 2006.

Fast, J. D., Allan, J., Bahreini, R., Craven, J., Emmons, L., Ferrare, R., Hayes, P. L., Hodzic, A., Holloway, J., Hostetler, C., Jimenez, J. L., Jonsson, H., Liu, S., Liu, Y., Metcalf, A., Middlebrook, A., Nowak, J., Pekour, M., Perring, A., Russell, L., Sedlacek, A., Seinfeld, J., Setyan, A., Shilling, J., Shrivastava, M., Springston, S., Song,
670   C., Subramanian, R., Taylor, J. W., Vinoj, V., Yang, Q., Zaveri, R. A., and Zhang, Q.: Modeling regional aerosol and aerosol precursor variability over California and its sensitivity to emissions and long-range transport during the 2010 CalNex and CARES campaigns, Atmos. Chem. Phys., 14, 10013-10060, https://doi.org/10.5194/acp-14-10013-2014, 2014.

Fiore, A. M., Levy II, H., and Jaffe, D. A.: North American isoprene influence on intercontinental ozone pollution,
675   Atmos. Chem. Phys., 11, 1697–1710, https://doi.org/10.5194/acp-11-1697-2011, 2011.

Fiore, A., Dentener, F. J., Wild, O., Cuvelier, C., Schultz, M. G., Hess, P., Textor, C., Schulz, M., Doherty, R. M., Horowitz, L. W., MacKenzie, I. A., Sanderson, M. G., Shindell, D. T., Stevenson, D. S., Szopa, S., Dingenen, R. V., Zeng, G., Atherton, C., Bergmann, D., Bey, I., Carmichael, G., Collins, W. J., Duncan, B. N., Faluvegi, G., Folberth, G., Gauss, M., Gong, S., Hauglustaine, D., Holloway, T., Isaksen, I. S. A., Jacob, D. J., Jonson, J. E.,
680   Kaminski, J. W., Keating, T. J., Lupu, A., Marmer, E., Montanaro, V., Park, R. J., Pitari, G., Pringle, K. J., Pyle, J. A., Schroeder, S., Vivanco, M. G., Wind, P., Wojcik, G., Wu, S., and Zuber, A.: Multimodel estimates of intercontinental source-receptor relationships for ozone pollution, J. Geophys. Res., 114, D04301, https://doi.org/10.1029/2008JD010816, 2009.

Fiore, A. M., West, J. J., Horowitz, L. W., Naik, V., and Schwarzkopf, M. D.: Characterizing the tropospheric
685   ozone response to methane emission controls and the benefits to climate and air quality, J. Geophys. Res., 113, D08-307,https://doi.org/10.1029/2007JD009162,2008.

Gao, M., Han, Z., Liu, Z., Li, M., Xin, J., Tao, Z., Li, J., Kang, J.-E., Huang, K., Dong, X., Zhuang, B., Li, S., Ge, B., Wu, Q., Cheng, Y., Wang, Y., Lee, H.-J., Kim, C.-H., Fu, J. S., Wang, T., Chin, M., Woo, J.-H., Zhang, Q., Wang, Z., and Carmichael, G. R.: Air quality and climate change, Topic 3 of the Model Inter-Comparison
690   Study for Asia Phase III (MICS-Asia III) – Part 1: Overview and model evaluation, Atmos. Chem. Phys., 18, 4859–4884, https://doi.org/10.5194/acp-18-4859-2018, 2018.

Georgiou, G. K., Christoudias, T., Proestos, Y., Kushta, J., Hadjinicolaou, P., and Lelieveld, J.: Air quality modelling in the summer over the eastern Mediterranean using WRF-Chem: chemistry and aerosol mechanism intercomparison, Atmos. Chem. Phys., 18, 1555–1571, https://doi.org/10.5194/acp-18-1555-2018, 2018.

695   Ghermandi, G., Fabbi, S., Veratti, G., Bigi, A., Teggi, S.: Estimate of Secondary NO_2 Levels at Two Urban Traffic Sites Using Observations and Modelling. Sustainability, 12, 7897. https://doi.org/10.3390/su12197897, 2020

Gómez-Navarro, J. J., Raible, C. C., and Dierer, S.: Sensitivity of the WRF model to PBL parametrisations and nesting techniques: evaluation of wind storms over complex terrain, Geosci. Model Dev., 8, 3349–3363, https://doi.org/10.5194/gmd-8-3349-2015, 2015.

700   Grell, G. A., Peckham, S. E., Schmitz, R., McKeen, S. A., Frost, G., Skamarock, W. C., and Eder, B.: Fully coupled online chemistry within the WRF model, Atmos. Environ., 39, 6957-6975, 2005.

Grewe, V., Tsati, E., Mertens, M., Frömming, C., and Jöckel, P.: Contribution of emissions to concentrations: the TAGGING 1.0 submodel based on the Modular Earth Submodel System (MESSy 2.52), Geosci. Model Dev., 10, 2615–2633, https://doi.org/10.5194/gmd-10-2615-2017, 2017.

705   Guenther, A. B., Jiang, X., Heald, C. L., Sakulyanontvittaya, T., Duhl, T., Emmons, L. K., & Wang, X.:. The Model of Emissions of Gases and Aerosols from Nature version 2.1 (MEGAN2.1): An extended and updated framework for modeling biogenic emissions. Geoscientific Model Development, 5(6), 1471–1492. https://doi.org/10.5194/gmd-5-1471-2012, 2012.

Guenther, A., Karl, T., Harley, P., Wiedinmyer, C., Palmer, P. I., and Geron, C.: Estimates of global terrestrial

710   isoprene emissions using MEGAN (Model of Emissions of Gases and Aerosols from Nature), Atmos. Chem. Phys., 6, 3181–3210, doi:10.5194/acp-6-3181-2006, 2006.

Guerova, G, and Jones, N.: A global model study of ozone enhancement during the August 2003 heat wave in Europe, Environ. Chem., 4, 285–292. doi:10.1071/EN07027, 2007.

Gong, C., Lei, Y., Ma, Y., Yue, X., and Liao, H.: Ozone–vegetation feedback through dry deposition and isoprene

715   emissions in a global chemistry–carbon–climate model, Atmos. Chem. Phys., 20, 3841–3857, https://doi.org/10.5194/acp-20-3841-2020, 2020.

Hong, S.-Y., Y. Noh, and J. Dudhia: A new vertical diffusion package with an explicit treatment of entrainment processes. Mon. Wea. Rev., 134, 2318–2341, doi: 10.1175/MWR3199.1., 2006

Iacono, M. J., Delamere, J. S., Mlawer, E. J., Shephard, M. W., Clough, S. A., and Collins, W. D.: Radiative

720   forcing by long-lived greenhouse gases: Calculations with the AER radiative transfer models, J. Geophys. Res., 113, D13103, doi:10.1029/2008JD009944, 2008.

Hoy, A., Hänsel, S., Skalak, S., Ustrnul, Z., and Bochníček, O.: The extreme European summer of 2015 in a long-term perspective,Int. J. Climatol., 37, 943–962, doi:10.1002/joc.4751, 2016.

Im, U., Bianconi, R., Solazzo, E., Kioutsioukis, I., Badia, A.,Balzarini, A., Baro, R., Bellasio, R., Giordano, L.,

725   Jimenez-Guerrero, P., Hirtl, M., Hodzic, A., Honzak, L., Jorba, O., Knote,C., Kuenen, J. J. P., Makar, P. A., Mandes-Groot, A., Neal,L., Perez, J. L., Pirovano, G., Pouliot, G., San Jose, R., Sav-age, N., Schroder, W., Sokhi, R. S., Syrakov, D., Torian, A.,Tucella, P., Werhahn, J., Wolke, R., Yahya, K., Zabkar, R.,Zhang, Y., Zhang, J., Hogrefe, C., and Galmarini, S.: Evaluation of operational on-lin-coupled regional air quality models over Europe and North America in the contex of AQMEII phase1. Part II: Particulate matter, Atmos. Environ., 115, 421–441,

730   https://doi.org/10.1016/j.atmosenv.2014.08.072, 2015.

Ionita, M., Tallaksen, L. M., Kingston, D. G., Stagge, J. H., Laaha, G., Van Lanen, H. A. J., Scholz, P., Chelcea, S. M., and Haslinger, K.: The European 2015 drought from a climatological perspective, Hydrol. Earth Syst. Sci., 21, 1397–1419, https://doi.org/10.5194/hess-21-1397-2017, 2017.

IPCC, 2012: Managing the Risks of Extreme Events and Disasters to Advance Climate Change Adaptation. A

735   Special Report of Working Groups I and II of the Intergovernmental Panel on Climate Change [Field, C.B., V.Barros, T.F. Stocker, D. Qin, D.J. Dokken, K.L. Ebi, M.D. Mastrandrea, K.J. Mach, G.-K. Plattner, S.K. Allen, M. Tignor, and P.M. Midgley (eds.)]. Cambridge University Press, Cambridge, United Kingdom and New York, NY, USA, 582pp., 2012

IPCC, 2018: Smith, K.R., A. Woodward, D. Campbell-Lendrum, D.D. Chadee, Y. Honda, Q. Liu, J.M. Olwoch,

740   B. Revich, and R. Sauerborn, 2014: Human health: impacts, adaptation, and co-benefits. In: Climate Change 2014: Impacts, Adaptation, and Vulnerability. Part A: Global and Sectoral Aspects. Contribution of Working Group II to the Fifth Assessment Report of the Intergovernmental Panel on Climate Change [Field, C.B., V.R. Barros, D.J. Dokken, K.J. Mach, M.D. Mastrandrea, T.E. Bilir, M. Chatterjee, K.L. Ebi, Y.O. Estrada, R.C. Genova, B. Girma, E.S. Kissel, A.N. Levy, S. MacCracken, P.R. Mastrandrea, and L.L. White (eds.)]. Cambridge

745   University Press, Cambridge, United Kingdom and New York, NY, USA, pp. 709-754., 2018

Jacob, D. J., and Winner, D.A.:. Effect of climate change on air quality. Atmospheric Environment 43(1): 51-63., 2009

Janssens-Maenhout, G., Crippa, M., Guizzardi, D., Dentener, F., Muntean, M., Pouliot, G., Keating, T., Zhang, Q., Kurokawa, J., Wankmüller, R., Denier van der Gon, H., Kuenen, J. J. P., Klimont, Z., Frost, G., Darras, S., Koffi, B., and Li, M.: HTAP_v2.2: a mosaic of regional and global emission grid maps for 2008 and 2010 to study hemispheric transport of air pollution, Atmos. Chem. Phys., 15, 11411–11432, https://doi.org/10.5194/acp-15-11411-2015, 2015.

Jiang, J., Aksoyoglu, S., Ciarelli, G., Oikonomakis, E., El-Haddad, I., Canonaco, F., O'Dowd, C., Ovadnevaite, J., Minguillón, M. C., Baltensperger, U., and Prévôt, A. S. H.: Effects of two different biogenic emission models on modelled ozone and aerosol concentrations in Europe, Atmos. Chem. Phys., 19, 3747–3768, https://doi.org/10.5194/acp-19-3747-2019, 2019.

Jiang, X., Guenther, A., Potosnak, M., Geron, C., Seco, R., Karl, T., Kim, S., Gu, L., Pallardy, S.: Isoprene emission response to drought and the impact on global atmospheric chemistry, Atmospheric Environment, 183, pp. 69-83., doi: 10.1016/j.atmosenv.2018.01.026, 2018

Jonson, J. E., Gauss, M., Schulz, M., Jalkanen, J.-P., and Fagerli, H.: Effects of global ship emissions on European air pollution levels, Atmospheric Chemistry and Physics Discussions, https://doi.org/10.5194/acp-2020-293, 2020

Otu-Larbi, F., Bolas, C. G., Ferracci, V., Staniaszek, Z., Jones, R. L., Malhi, Y., Harris, N.R.P., Wild, O., Ashworth, K.: Modelling the effect of the 2018 summer heatwave and drought on isoprene emissions in a UK woodland. *Global Change Biology*, 26(4), 2320– 2335, https://doi.org/10.1111/gcb.14963,2020

Jonson, J. E., Schulz, M., Emmons, L., Flemming, J., Henze, D., Sudo, K., Tronstad Lund, M., Lin, M., Benedictow, A., Koffi, B., Dentener, F., Keating, T., Kivi, R., and Davila, Y.: The effects of intercontinental emission sources on European air pollution levels, Atmos. Chem. Phys., 18, 13655–13672, https://doi.org/10.5194/acp-18-13655-2018, 2018.

Kain, J. S.: The Kain-Fritsch convective parameterization: An update. J. Appl. Meteor., 43, 170-181., 2004

Kalabokas, P. D., Cammas, J.-P., Thouret, V., Volz-Thomas, A., Boulanger, D., and Repapis, C. C.: Examination of the atmospheric conditions associated with high and low summer ozone levels in the lower troposphere over the eastern Mediterranean, Atmos. Chem. Phys., 13, 10339–10352, https://doi.org/10.5194/acp-13-10339-2013, 2013.

Karlický, J., Huszár, P., Nováková, T., Belda, M., Švábik, F., Ďoubalová, J., and Halenka, T.: The "urban meteorology island": a multi-model ensemble analysis, Atmos. Chem. Phys., 20, 15061–15077, https://doi.org/10.5194/acp-20-15061-2020, 2020.

Kaspar, F., Müller-Westermeier, G., Penda, E., Mächel, H., Zimmermann, K., Kaiser-Weiss, A., and Deutschländer, T.: Monitoring of climate change in Germany – data, products and services of Germany's National Climate Data Centre, Adv. Sci. Res., 10, 99–106, https://doi.org/10.5194/asr-10-99-2013, 2013.

Kehler-Poljak, G., Telišman Prtenjak, M., Kvakić, M., Šariri, K., and Zečenaj, Z.: Interaction of Sea Breeze and Deep Convection over the Northeastern Adriatic Coast: An Analysis of Sensitivity Experiments Using a High-Resolution Mesoscale Model. Pure Appl. Geophys. 174, 4197–4224 (2017), https://doi.org/10.1007/s00024-017-1607-x.,2017

Kryza, M., Werner, M., Dudek, J., and Dore, A.J.: The Effect of Emission Inventory on Modelling of Seasonal Exposure Metrics of Particulate Matter and Ozone with the WRF-Chem Model for Poland. Sustainability, 12(13):5414, https://doi.org/10.3390/su12135414, 2020

Kuenen, J. J. P., Visschedijk, A. J. H., Jozwicka, M., and Denier van der Gon, H. A. C.: TNO-MACC_II emission inventory; a multi-year (2003–2009) consistent high-resolution European emission inventory for air quality modelling, Atmos. Chem. Phys., 14, 10963–10976, https://doi.org/10.5194/acp-14-10963-2014, 2014.

790   Kuik, F., Lauer, A., Churkina, G., Denier van der Gon, H. A. C., Fenner, D., Mar, K. A., and Butler, T. M.: Air quality modelling in the Berlin–Brandenburg region using WRF-Chem v3.7.1: sensitivity to resolution of model grid and input data, Geosci. Model Dev., 9, 4339–4363, https://doi.org/10.5194/gmd-9-4339-2016, 2016.

Kuik, F., Kerschbaumer, A., Lauer, A., Lupascu, A., von Schneidemesser, E., and Butler, T. M.: Top–down quantification of NO_x emissions from traffic in an urban area using a high-resolution regional atmospheric chemistry model, Atmos. Chem. Phys., 18, 8203–8225, https://doi.org/10.5194/acp-18-8203-2018, 2018.

795

Kushta J., Georgiou G.K., Proestos Y., Christoudias T., Thunis P., Savvides C., Papadopoulos C., Lelieveld J.: Evaluation of EU air quality standards through modeling and the FAIRMODE benchmarking methodology. Air Qual Atmos Health 12, 73–86. https://doi.org/10.1007/s11869-018-0631-z, 2019

Hu, X.-M., Klein, P. M., and Xue, M.: Evaluation of the updated YSU planetary boundary layer scheme within

800   WRF for wind resource and air quality assessments, J. Geophys. Res. Atmos., 118, 10,490–10,505, doi:10.1002/jgrd.50823, 2013

Lee, K.-Y., Kwak, K.-H., Ryu, Y.-H., Lee, S.-H., and Baik, J.-J.: Impacts of biogenic isoprene emission on ozone air quality in the Seoul metropolitan area, Atmos. Environ., 96, 209–219, https://doi.org/10.1016/j.atmosenv.2014.07.036, 2014.

805   Lin, M., Horowitz, L., Paulot, F., Malyshev, S., Shevliakova, E., Finco, A., Gerosa, G., Kubistin, D., and Pilegaard, K.:Vegetation feedbacks during drought exacerbate ozone air pollution extremes in Europe, Nat. Clim. Change, 10, p. 791, 10.1038/s41558-020-0839-4., 2020.

Lin, M., Malyshev, S., Shevliakova, E., Paulot, F., Horowitz, L. W., Fares, S., Mikkelsen, T. N., and Zhang, L.: Sensitivity of ozone dry deposition to ecosystem-atmosphere interactions: A critical appraisal of observations and

810   simulations. Global Biogeochemical Cycles, 33, 1264–1288, https://doi.org/10.1029/2018GB006157, 2019.

Lin, C.-Y. C., Jacob, D. J., and Fiore, A. M.: Trends in exceedances of the ozone air quality standard in the continental United States, 1980–1998, Atmos. Environ., 35, 3217–3228, 2001.

Lu, X., Ye, X., Zhou, M., Zhao, Y., Weng, H., Kong, H., Li, K., Gao, M., Zheng, B., Lin, J., Zhou, F., Zhang, Q., Wu, D., Zhang, L., Zhang, Y.: The underappreciated role of agricultural soil nitrogen oxide emissions in ozone

815   pollution regulation in North China. Nat Commun 12, 5021, https://doi.org/10.1038/s41467-021-25147-9, 2021

Lupaşcu, A. and Butler, T.: Source attribution of European surface O_3 using a tagged O_3 mechanism, Atmos. Chem. Phys., 19, 14535–14558, https://doi.org/10.5194/acp-19-14535-2019, 2019.

Mailler, S., Khvorostyanov, D., and Menut, L.: Impact of the vertical emission profiles on background gas-phase pollution simulated from the EMEP emissions over Europe, Atmos. Chem. Phys., 13, 5987–5998,

820   https://doi.org/10.5194/acp-13-5987-2013, 2013.

Meehl GA, Tebaldi C, Tilmes S, Lamarque JF, Bates S, Pendergrass A, et al. Future heat waves and surface ozone. Environ Res Lett.;13(6):9, https://doi.org/10.1088/1748-9326/aabcdc., 2018.

Mertens, M., Kerkweg, A., Grewe, V., Jöckel, P., and Sausen, R.: Attributing ozone and its precursors to land transport emissions in Europe and Germany, Atmos. Chem. Phys., 20, 7843–7873, https://doi.org/10.5194/acp-

825   20-7843-2020, 2020.

Morrison, H., Thompson, G., and Tatarskii, V.: Impact of cloud microphysics on the development of trailing stratiform precipitation in a simulated squall line: comparison of one- and two-moment schemes. Monthly Weather Review, 137, 991–1007, doi:10.1175/2008MWR2556.1, 2009.

Ordóñez, C., Elguindi, N., Stein, O., Huijnen, V., Flemming, J., Inness, A., Flentje, H., Katragkou, E., Moinat, P., Peuch, V.-H., Segers, A., Thouret, V., Athier, G., van Weele, M., Zerefos, C. S., Cammas, J.-P., and Schultz, M. G.: Global model simulations of air pollution during the 2003 European heat wave, Atmos. Chem. Phys., 10, 789-815, doi:10.5194/acp-10-789-2010, 2010.

Oikonomakis, E., Aksoyoglu, S., Ciarelli, G., Baltensperger, U., and Prévôt, A. S. H.: Low modeled ozone production suggests underestimation of precursor emissions (especially NO_x) in Europe, Atmos. Chem. Phys., 18, 2175–2198, https://doi.org/10.5194/acp-18-2175-2018, 2018.

Otero, N., Jurado, O. E., Butler, T., and Rust, H. W.: The impact of atmospheric blocking on the compounding effect of ozone pollution and temperature: a copula-based approach, Atmos. Chem. Phys., 22, 1905–1919, https://doi.org/10.5194/acp-22-1905-2022, 2022.

Otero Felipe, N., Rust, H. W., and Butler, T. M.: Temperature dependence of tropospheric ozone under NOx reductions over Germany. Atmospheric Environment, 253: 118334. doi:10.1016/j.atmosenv.2021.118334., 2021

Otero, N., Sillmann, J., Mar, K. A., Rust, H. W., Solberg, S., Andersson, C., Engardt, M., Bergström, R., Bessagnet, B., Colette, A., Couvidat, F., Cuvelier, C., Tsyro, S., Fagerli, H., Schaap, M., Manders, A., Mircea, M., Briganti, G., Cappelletti, A., Adani, M., D'Isidoro, M., Pay, M.-T., Theobald, M., Vivanco, M. G., Wind, P., Ojha, N., Raffort, V., and Butler, T.: A multi-model comparison of meteorological drivers of surface ozone over Europe, Atmos. Chem. Phys., 18, 12269–12288, https://doi.org/10.5194/acp-18-12269-2018, 2018.

Otero, N., Sillmann, J., Schnell, J. L., Rust, H. W., and Butler, T.: Synoptic and meteorological drivers of extreme ozone concentrations over Europe, Environ. Res. Lett., 11, 024005, doi:10.1088/1748-9326/11/2/024005, 2016

Orth, R., Zscheischler, J., and Seneviratne, S. I.: Record dry summer in 2015 challenges precipitation projections in Central Europe. Scientific Reports, 6: 28334. doi:10.1038/srep28334, 2016

Pay, M. T., Gangoiti, G., Guevara, M., Napelenok, S., Querol, X., Jorba, O., and Pérez García-Pando, C.: Ozone source apportionment during peak summer events over southwestern Europe, Atmos. Chem. Phys., 19, 5467–5494, https://doi.org/10.5194/acp-19-5467-2019, 2019.

Pfister, G. G., Emmons, L. K., Hess, P. G., Lamarque, J.-F., Orlando, J. J., Walters, S., Guenther, A., Palmer, P. I., and Lawrence, P. J.: Contribution of isoprene to chemical budgets: A model tracer study with the NCAR CTM MOZART-4, J. Geophys. Res., 113, D05308, doi:10.1029/2007JD008948, 2008.

Pirovano, G., Balzarini, A., Bessagnet, B., Emery, C., Kallos, G., Meleux, F., Mitsakou, C., Nopmongcol, U., Riva, G., and Yarwood, G.: Investigating impacts of chemistry and transport model formulation on model performance at European scale, Atmos. Environ., 53, 93–109, https://doi.org/10.1016/j.atmosenv.2011.12.052, 2012.

Porter, W. C., Heald, C. L., Cooley, D., and Russell, B.: Investigating the observed sensitivities of air-quality extremes to meteorological drivers via quantile regression, Atmos. Chem. Phys., 15, 10349–10366, https://doi.org/10.5194/acp-15-10349-2015, 2015.

Pusede, S.E., Steiner, A.L., and Cohen, R.C.: Temperature and recent trends in the chemistry of continental surface ozone. Chem Rev 115:3898–3918, https://doi.org/10.1021/cr5006815, 2015

Qu, Y., An, J., and Li, J.: Synergistic impacts of anthropogenic and biogenic emissions on summer surface O_3 in East Asia, J. Environ. Sci., 25, 520–530, https://doi.org/10.1016/s1001-0742(12)60069-2, 2013.

J.H. Rydsaaa, F. Stordala, G. Gerosab, A. Fincob, Ø. Hodnebrog Evaluating stomatal ozone fluxes in WRF-Chem: Comparing ozone uptake in Mediterranean ecosystems, Atmospheric Environment, 143, pp. 237-248, https://doi.org/10.1016/j.atmosenv.2016.08.057, 2016

870   Schnell, J.L., and Prather, M.J.: Co-occurrence of extremes in surface ozone, particulate matter, and temperature over eastern North America. Proc Natl Acad Sci.;114(11):2854, https://doi.org/10.1073/pnas.1614453114, 2017

Wang, Y., Xie, Y., Dong, W., Ming, Y., Wang, J., and Shen, L.: Adverse effects of increasing drought on air quality via natural processes, Atmos. Chem. Phys., 17, 12827–12843, https://doi.org/10.5194/acp-17-12827-2017, 2017.

875   Shen, L., L. J. Mickley, E. Gilleland:, Impact of increasing heat waves on U.S. ozone episodes in the 2050s: Results from a multimodel analysis using extreme value theory, Geophys. Res. Lett., 43, 4017–4025, doi:10.1002/2016GL068432, 2016.

Sillmann, Jana & Aunan, Kristin & Emberson, Lisa & Büker, Patrick & van Oort, Bob & O'Neill, Connie & Otero, Noelia & Pandey, Divya & Brisebois, Anouk. (2021). Combined impacts of climate and air pollution on human

880   health and agricultural productivity. Environmental Research Letters. 16. 10.1088/1748-9326/ac1df8.

Sillman, S., and He, D.: Some theoretical results concerning O_3-NO_x-VOC chemistry and NO_x-VOC indicators. J. Geophys. Res. D22:4659, doi: 10.1029/2001JD001123, 2002

Sillman, S.: The use of NO_y, H_2O_2, and HNO_3 as indicator for the NO_x-hydrocarbon sensitivity in urban locations, *J. Geophys., Res.*, 100, 14,175– 14,188, https://doi.org/10.1029/94JD02953. 1995

885   Simpson, D.: Biogenic emissions in Europe 2: Implications for ozone control strategies. J. Geophys. Res., 100(D11):22891–22906, 1995.

Simpson, D., Guenther, A., Hewitt, C.N., and Steinbrecher, R.: Biogenic emissions in Europe 1. Estimates and uncertainties. J. Geophys. Res., 100(D11):22875–22890, 1995

Stanier, C.O., Pierce, R.B., Abdi-Oskouei, M., Adelman, Z.E., Al-Saadi, J., Alwe, H.D., Bertram, T.H.,

890   Carmichael, G.R., Christiansen, M.B., Cleary, P.A., Czarnetzki, A.C., Dickens, A.F., Fuoco, M.A., Hughes, D.D. , Hupy, J.P., Janz, S.J., Judd, L.M., Kenski, D., Kowalewski, M.G., Long, R.W., Millet, D.B., Novak, G., Roozitalab, B., Shaw, S.L., Stone, E.A., Szykman, J., Valin, L., Vermeuel, M., Wagner, T.J., and Whitehill, A.R.: Overview of The lake Michigan ozone study 2017**.** Bull. Am. Meteorol. Soc. (2021), 102(12), pp. E2207-E2225, 10.1175/BAMS-D-20-0061.1., 2021

895   Struzewska, J. and Kaminski, J. W.: Formation and transport of photooxidants over Europe during the July 2006 heat wave – observations and GEM-AQ model simulations, Atmos. Chem. Phys., 8, 721-736, doi:10.5194/acp-8-721-2008, 2008.

Sun, J., Shen, Z., Wang, R., Li, G., Zhang, Y., Zhang, B., He, K,. Tang, Z., Xu, H., Qu, L., Sai Hang Ho, S., Liu, S,. and Cao, J.: A comprehensive study on ozone pollution in a megacity in North China Plain during summertime:

900   Observations, source attributions and ozone sensitivity, Environ Int., 146:106279. doi: 10.1016/j.envint.2020.106279. PMID: 33276317, 2021

Tagaris, E., Sotiropoulou, R., Gounaris, N., Andronopoulos, S., and Vlachogiannis, D.: Impact of biogenic emissions on ozone and fine particles over Europe: Comparing effects of temperature increase and a potential anthropogenic NOx emissions abatement strategy, Atmos. Environ., 98, 214–223,

905   https://doi.org/10.1016/j.atmosenv.2014.08.056, 2014.

Tao, Z., Chin, M., Gao, M., Kucsera, T., Kim, D., Bian, H., Kurokawa, J., Wang, Y., Liu, Z., Carmichael, G. R., Wang, Z., and Akimoto, H.: Evaluation of NU-WRF model performance on air quality simulation under various

model resolutions – an investigation within the framework of MICS-Asia Phase III, Atmos. Chem. Phys., 20, 2319–2339, https://doi.org/10.5194/acp-20-2319-2020, 2020.

910 Solazzo, E., Bianconi, R., Hogrefe, C., Curci, G., Tuccella, P., Alyuz, U., Balzarini, A., Baró, R., Bellasio, R., Bieser, J., Brandt, J., Christensen, J. H., Colette, A., Francis, X., Fraser, A., Vivanco, M. G., Jiménez-Guerrero, P., Im, U., Manders, A., Nopmongcol, U., Kitwiroon, N., Pirovano, G., Pozzoli, L., Prank, M., Sokhi, R. S., Unal, A., Yarwood, G., and Galmarini, S.: Evaluation and error apportionment of an ensemble of atmospheric chemistry transport modeling systems: multivariable temporal and spatial breakdown, Atmos. Chem. Phys., 17, 3001–3054,

915 https://doi.org/10.5194/acp-17-3001-2017, 2017.

Tilmes, S., Lamarque, J.-F., Emmons, L. K., Kinnison, D. E., Ma, P.-L., Liu, X., Ghan, S., Bardeen, C., Arnold, S., Deeter, M., Vitt, F., Ryerson, T., Elkins, J. W., Moore, F., Spackman, J. R., and Val Martin, M.: Description and evaluation of tropospheric chemistry and aerosols in the Community Earth System Model (CESM1.2), Geosci. Model Dev., 8, 1395–1426, https://doi.org/10.5194/gmd-8-1395-2015, 2015.

920 Tuccella, P., Curci, G., Visconti, G., Bessagnet, B., and Menut,L.: Modeling of gas and aerosol with WRF/Chem over Europe: Evaluation and sensitivity study, J. Geophys. Res., 117, D03303,doi:10.1029/2011JD016302, 2012.

Turnipseed, A.A., Burns, S.P., Moore, D.J.P., Hu, J., Guenther, A.B. and Monson, R.K.:.Controls over ozone deposition to a high elevation subalpine forest. Agricultural and Forest Meteorology 149, 1447-1459, https://doi.org/10.1016/j.agrformet.2009.04.001,2009

925 Shen, L., Mickley, L. J. and Gilleland, E.: Impact of increasing heat waves on U.S. ozone episodes in the 2050s: Results from a multimodel analysis using extreme value theory, Geophys. Res. Lett., 43, 4017–4025, doi:10.1002/2016GL068432, 2016

Turnock, S. T., Wild, O., Sellar, A., and O'Connor, F. M.: 300 years of tropospheric ozone changes using CMIP6 scenarios with a parameterised approach, Atmospheric Environment, 213, 686–698, doi: 10.1016/j.atmosenv.2019.07.001, 2019.

930 Turnock, S. T., Wild, O., Dentener, F. J., Davila, Y., Emmons, L. K., Flemming, J., Folberth, G. A., Henze, D. K., Jonson, J. E., Keating, T. J., Kengo, S., Lin, M., Lund, M., Tilmes, S., and O'Connor, F. M.: The impact of future emission policies on tropospheric ozone using a parameterised approach, Atmos. Chem. Phys., 18, 8953–8978, https://doi.org/10.5194/acp-18-8953-2018, 2018.

935 Vautard, R., Honoré, C., Beekmann, M., and Rouil, L.: Simulation of ozone during the August 2003 heat wave and emission control scenarios, Atmos. Environ., 39, 2957–2967, 2005.

Vieno, M., Dore, A. J., Stevenson, D. S., Doherty, R., Heal, M. R., Reis, S., Hallsworth, S., Tarrason, L., Wind, P., Fowler, D., Simpson, D., and Sutton, M. A.: Modelling surface ozone during the 2003 heat-wave in the UK, Atmos. Chem. Phys., 10, 7963-7978, doi:10.5194/acp-10-7963-2010, 2010.

940 Visser, A. J., Boersma, K. F., Ganzeveld, L. N., and Krol, M. C.: European NO_x emissions in WRF-Chem derived from OMI: impacts on summertime surface ozone, Atmos. Chem. Phys., 19, 11821–11841, https://doi.org/10.5194/acp-19-11821-2019, 2019.

Wang, Y.; Jacob, D. J. Anthropogenic forcing on tropospheric ozone and OH since preindustrial times,. J. Geophys. Res, 103, 31123−31135. https://doi.org/10.1029/1998JD100004., 1998

945 Wiedinmyer, C., Akagi, S. K., Yokelson, R. J., Emmons, L. K., Al-Saadi, J. A., Orlando, J. J., and Soja, A. J.: The Fire INventory from NCAR (FINN): a high resolution global model to estimate the emissions from open burning, Geosci. Model Dev., 4, 625–641, https://doi.org/10.5194/gmd-4-625-2011, 2011.

West, J.J., and Fiore, A.M.: Management of tropospheric ozone by reducing methane emissions. *Environ. Sci. Technol.*, **39**, 4685 -4691, https://doi.org/10.1021/es048629f., 2005

950 Wesely, M.L., Parameterization of surface resistances to gaseous dry deposition in regional-scale numerical models, 757Atmospheric Environment, 23, 1293-1304, 1989.

Wyszogrodzki, A., Liu, Y., Jacobs, N., Childs, P., Zhang, Y., Roux, G., & Warner, T. T.: Analysis of the surface temperature and wind forecast errors of the NCAR-AirDat operational CONUS 4-km WRF forecasting system. Meteorology And Atmospheric Physics, 122, 125-143. doi:10.1007/s00703-013-0281-5, 2013

955 Zscheischler, J., and Fischer, E. M.: The record-breaking compound hot and dry 2018 growing season in Germany. Weather and Climate Extremes, 29, 100 270, doi:10.1016/j.wace.2020.100270, 2020

Zhang, R., Cohan, A., Biazar, A. P., and Cohan, D. S.: Source apportionment of biogenic contributions to ozone formation over the United States, Atmos. Environ., 164, 8–19, https://doi.org/10.1016/j.atmosenv.2017.05.044, 2017.

960 Zhao, C., Huang, M., Fast, J. D., Berg, L. K., Qian, Y., Guenther, A., Gu, D., Shrivastava, M., Liu, Y., Walters, S., Pfister, G., Jin, J., Shilling, J. E., and Warneke, C.: Sensitivity of biogenic volatile organic compounds to land surface parameterizations and vegetation distributions in California, Geosci. Model Dev., 9, 1959–1976, https://doi.org/10.5194/gmd-9-1959-2016, 2016.

965

970

975

980

985

Table 1. List of tagged European source regions for the NOx tagging mechanism

Category	Acronym	List of countries
European source regions	MBS	The Mediterranean, and Black Seas
	BNS	Baltic, and North Seas
	CEN	Austria, Hungary, Czech Republic, Slovakia, Estonia, Latvia, Lithuania, Poland
	ITS	Italy, Malta, and Switzerland
	SEE	Bulgaria, Romania, Moldavia, Albania, Slovenia, Croatia, Serbia, Montenegro, Macedonia, Greece, and Cyprus
	IBE	Spain, and Portugal
	UKI	The United Kingdom, and Ireland
	GER	Germany (without Berlin)
	BER	Berlin
	BNL	Belgium, Netherland, Luxembourg
	SCA	Finland, Norway, Sweden, Denmark, and Island
	FRA	France
	RBT	Russia, Belarus, Ukraine, Turkey, Azerbaijan, Armenia, and Georgia
HTAP2	ASI	Chemical boundary condition of modeled species coming from Asia
	NAM	Chemical boundary condition of modeled species coming from North America
	OCN	Chemical boundary condition of modeled species coming from shipping activities
	RST	Chemical boundary condition of modeled species coming from rest of the world
Global	BIO	Biogenic
	BMB	Biomass burning
	LGT	Lightning
	STR	Stratospheric O_3

990

995

1000 **Table 2.** Observed mean and simulation summary statistics for meteorological parameters. The bias, normalized mean bias (NMB), correlation coefficient (r), and index of agreement (IOA) are calculated between simulated and observed meteorological parameters at the DWD stations during the 6 – 13 August 2015 period.

Variable name	Observed mean	Bias	NMB (%)	r	IOA
2m temperature	22.9	-0.7	-0.3	0.86	0.90
T2MAX	28.5	-1.1	-0.3	0.42	0.56
Relative humidity	65.7	9.5	14.5	0.65	0.76
Pressure	984.01	4.1	0.4	0.91	0.98
Mean sea level pressure	1017.1	0.8	0.07	0.96	0.96
Wind speed	2.9	1.0	35.2	0.47	0.64
Wind direction	178.29	11.1	6.6	0.47	0.73

Table 3. Observed mean and simulation summary statistics for meteorological parameters. The bias, normalized
1005 mean bias (NMB), correlation coefficient (r), and index of agreement (IOA) are calculated between simulated and observed meteorological parameters at the DWD stations during the 1 – 8 August 2018 period.

Variable name	Observed mean	Bias	NMB (%)	r	IOA
2m temperature	23.9	-0.9	-0.2	0.84	0.86
T2MAX	30.4	-1.4	-0.5	0.22	0.28
Relative humidity	58.7	12.1	20.1	0.67	0.75
Pressure	984.5	4.3	0.4	0.91	0.92
Mean sea level pressure	1017.1	1.1	0,1	0.98	0.97
Wind speed	2.8	0.9	31.6	0.49	0.65
Wind direction	190.1	11.6	6.1	0.41	0.69

1010

1015

1020 **Table 4**. Observed mean and simulation summary statistics for NO$_2$, NO$_x$, O$_3$ and MDA8 O$_3$ concentrations. The bias, normalized mean bias (NMB), correlation coefficient (r), and index of agreement (IOA) are calculated between simulated and observed concentrations at the German "background" (all), "urban and suburban background" (ub) and "rural" (rb) stations during the 6 – 13 August 2015 period

Variable name	Observed mean (µg/m3)	Bias	NMB (%)	r	IOA
NO$_2$ (all)	13.5	-3.0	-22.3	0.39	0.59
NO$_x$ (all)	15.8	-4.7	-30.2	0.36	0.52
O$_3$ (all)	101.4	2.3	2.3	0.69	0.79
MDA8 O$_3$ (all)	128.7	-4.3	-3.3	0.74	0.82
NO$_2$ (rb)	7.1	0.4	6.3	0.12	0.58
NO$_x$ (rb)	7.9	-0.1	-1.6	0.11	0.54
O$_3$ (rb)	101.6	2.1	2.1	0.48	0.79
MDA8 O$_3$ (rb)	130.6	-7.8	-6.0	0.59	0.81
NO$_2$ (ub)	18.3	-5.6	-30.5	0.1	0.55
NO$_x$ (ub)	21.6	-8.3	-38.2	0.08	0.49
O$_3$ (ub)	95.4	13.4	14.0	0.41	0.67
MDA8 O$_3$ (ub)	127.72	-2.5	-1.96	0.56	0.83

1025 **Table 5.** Observed mean and simulation summary statistics for NO$_2$, NO$_x$, O$_3$ and MDA8 O$_3$ concentrations. The bias, normalized mean bias (NMB), correlation coefficient (r), and index of agreement (IOA) are calculated between simulated and observed concentrations at the German "background" (all), "urban and suburban background" (ub) and "rural" (rb) stations during the 1 – 8 August 2018 period

Variable name	Observed mean (µg/m3)	Bias	NMB (%)	R	IOA
NO$_2$ (all)	12.8	-1.7	-14.0	0.43	0.65
NO$_x$ (all)	14.9	-2.5	-16.5	0.37	0.61
O$_3$ (all)	96.9	-0.9	-0.9	0.62	0.74
MDA8 O$_3$ (all)	130.5	-12.5	-9.7	0.66	0.73
NO$_2$ (rb)	6.7	1.0	14.9	0.13	0.58
NO$_x$ (rb)	7.8	0.5	6.7	0.09	0.55
O$_3$ (rb)	103.5	-6.9	-6.8	0.39	0.75
MDA8 O$_3$ (rb)	130.4	-15.6	-11.9	0.48	0.74
NO$_2$ (ub)	16.7	-4.2	-21.6	0.14	0.61
NO$_x$ (ub)	18.7	-4.0	-21.6	0.10	0.57
O$_3$ (ub)	91.43	4.2	4.6	0.39	0.74
MDA8 O$_3$ (ub)	128.8	-11.1	-8.6	0.40	0.73

1030

Table 6. Percentage of stations in each day ~~which~~ that exceed~~s~~ the daily MDA8 O$_3$ target value during the 6 – 13 August 2015 and 1 – 8 August 2018 periods

2015								
Date	06 Aug.	07 Aug.	08 Aug.	09 Aug.	10 Aug.	11 Aug.	12 Aug.	13 Aug.
% of observed exceedances	90	82	58	35	55	57	50	69
% of modeled exceedances	91	82	59	30	40	42	44	46
2018								
Date	01 Aug.	02 Aug.	03 Aug.	04 Aug.	05 Aug.	06 Aug.	07 Aug.	08 Aug.
% of observed exceedances	49	80	92	73	19	49	89	58
% of modeled exceedances	48	60	66	41	9	15	63	48

1035

1040

1045

1050

1055

1060

Table 7. List of selected stations

Acronym	State	Station code	Station name	Station type
BE	Berlin	DEBE062	Berlin Frohnau	Background rural
BB	Brandenburg	DEBB086	Blankenfelde-Mahlow	Background suburban
BW	Baden-Württemberg	DEBW013	Stuttgart-Bad Cannstatt	Background urban
BY	Bavaria	DEBY093	Sulzbach-Rosenberg/Lohe	Background suburban
HE	Hesse	DEHE022	Wiesbaden-Süd	Background urban
MV	Mecklenburg-Vorpommern	DEMV026	Garz	Background rural
NI	Lower Saxony	DENI052	Allertal	Background suburban
NW	North Rhine-Westphalia	DENW081	Borken-Gemen	Background rural
RP	Rhineland-Palatinate	DERP022	Bad Kreuznach	Background urban
SH	Schleswig-Holstein	DESH015	Itzehoe	Background suburban
SL	Saarland	DESL019	Biringen	Background rural
SN	Saxony	DESN059	Leipzig-West	Background suburban
ST	Saxony-Anhalt	DEST104	Domäne Bobbe	Background rural
TH	Thuringia	DETH020	Erfurt	Background urban

1065
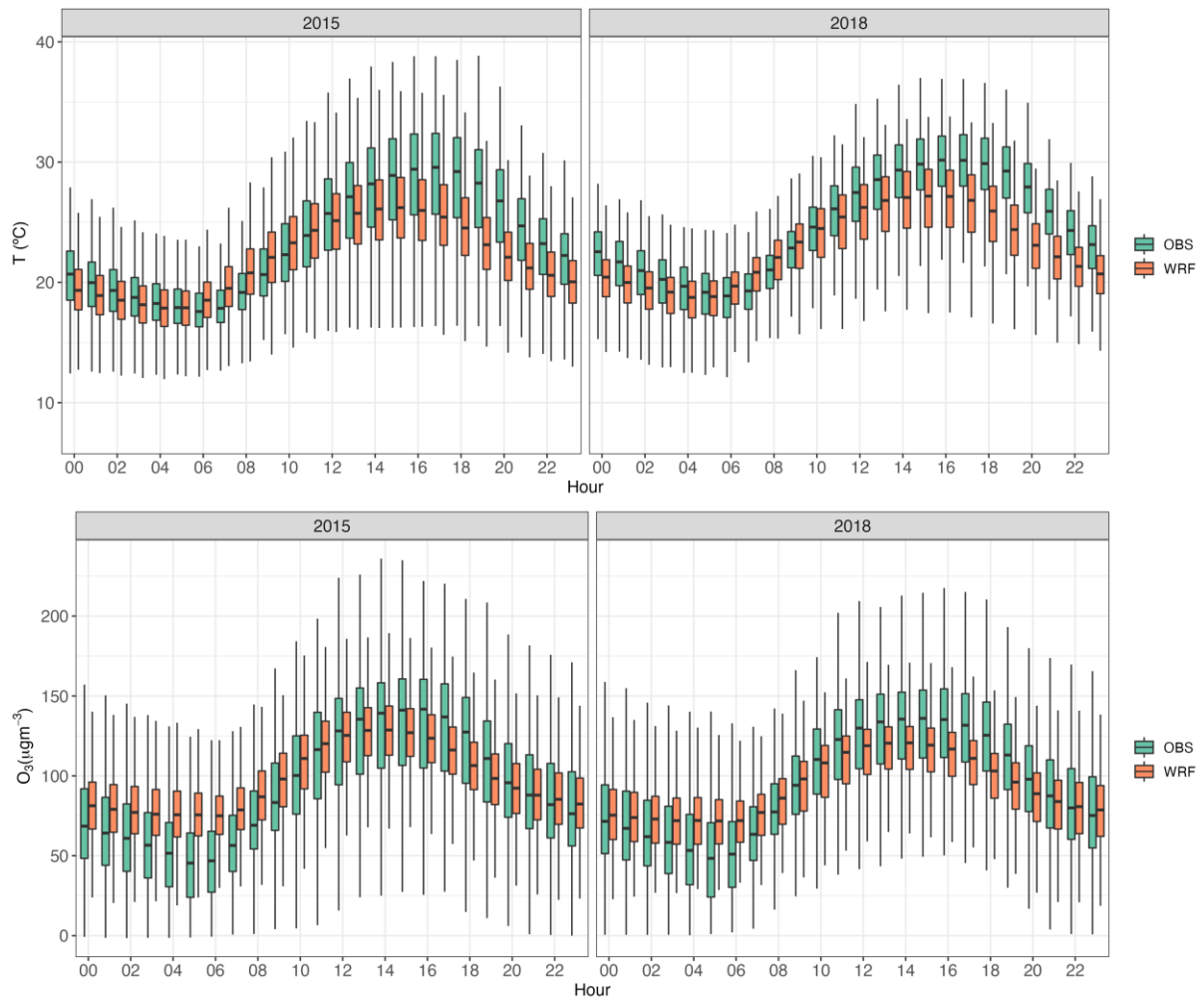
Figure 1. Observed and simulated diel percentile for temperature and O₃ over the analyzed periods at the German "background" stations. Note that the "OBS" temperature is given by ERA5 temperature extracted at the German background station locations. Vertical lines denote 5th and 95th percentiles, boxes denote 25th and 75th percentiles, and the black line denotes the 50th percentiles.
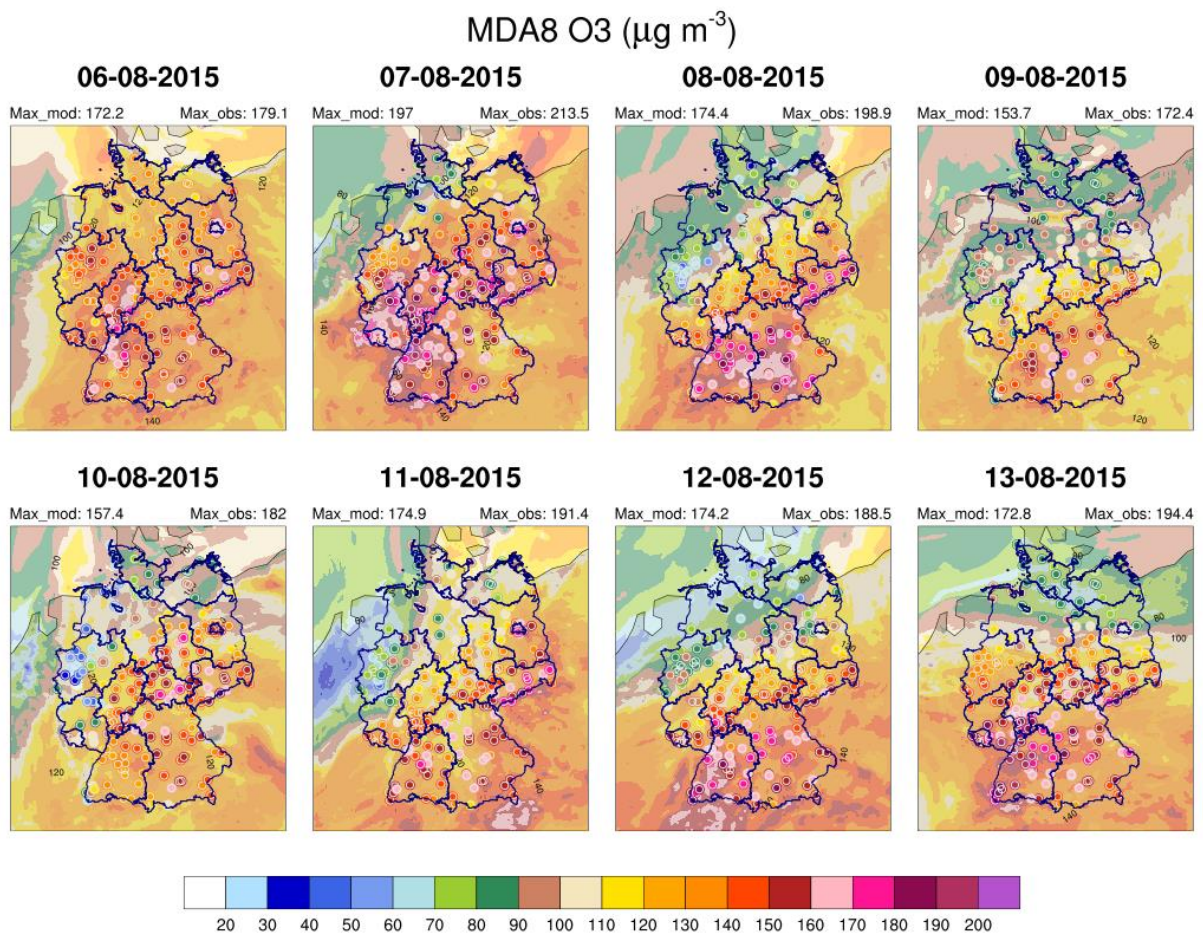
Figure 2. Daily surface MDA8 O_3 ($\mu g/m^3$) for the 6 – 13 August 2015 period. Color dots represent the observed MDA8 O_3 concentrations at the German "background" stations.
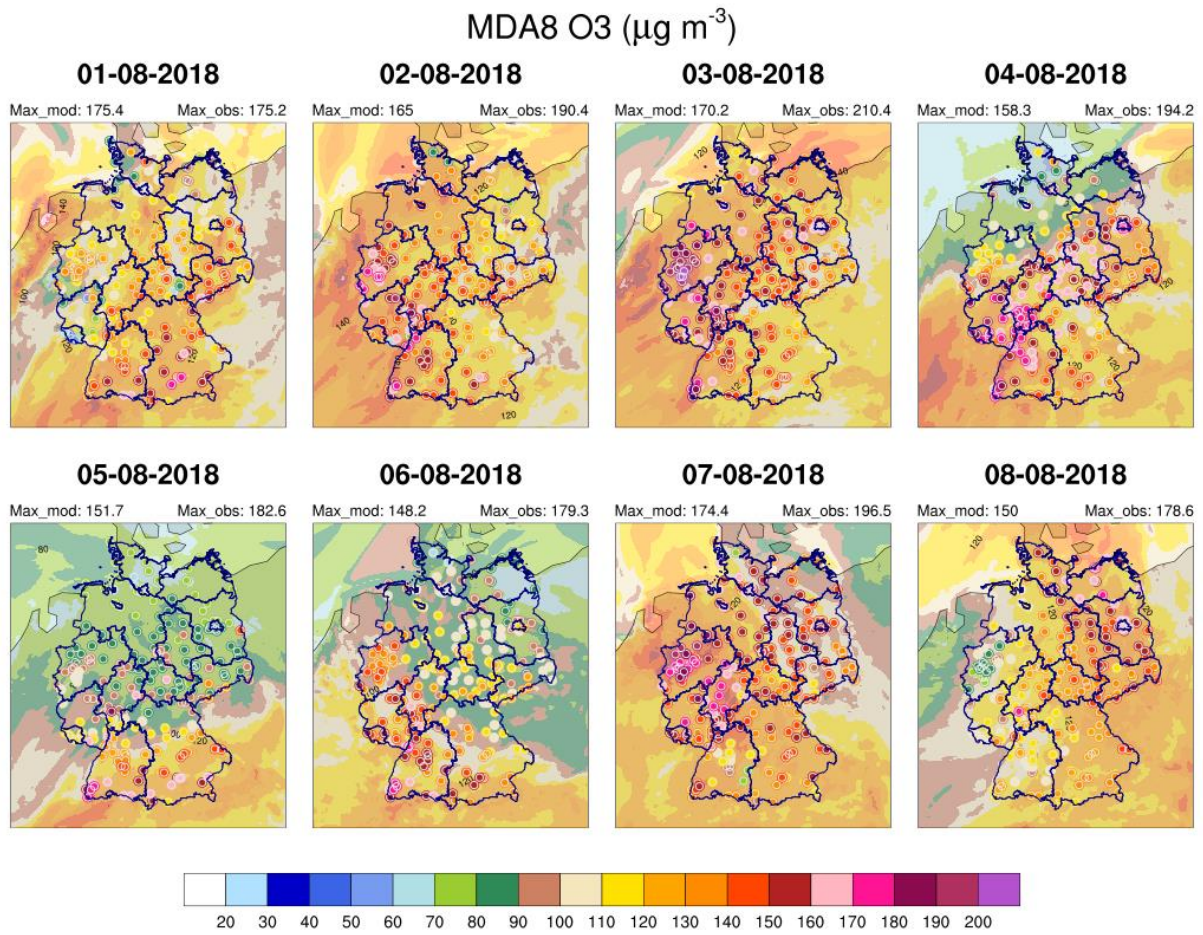
Figure 3. Daily surface MDA8 O₃ (μg/m³) for the 1 – 8 August 2018 period. Color dots represent the observed MDA8 O₃ concentrations at the German "background" stations.
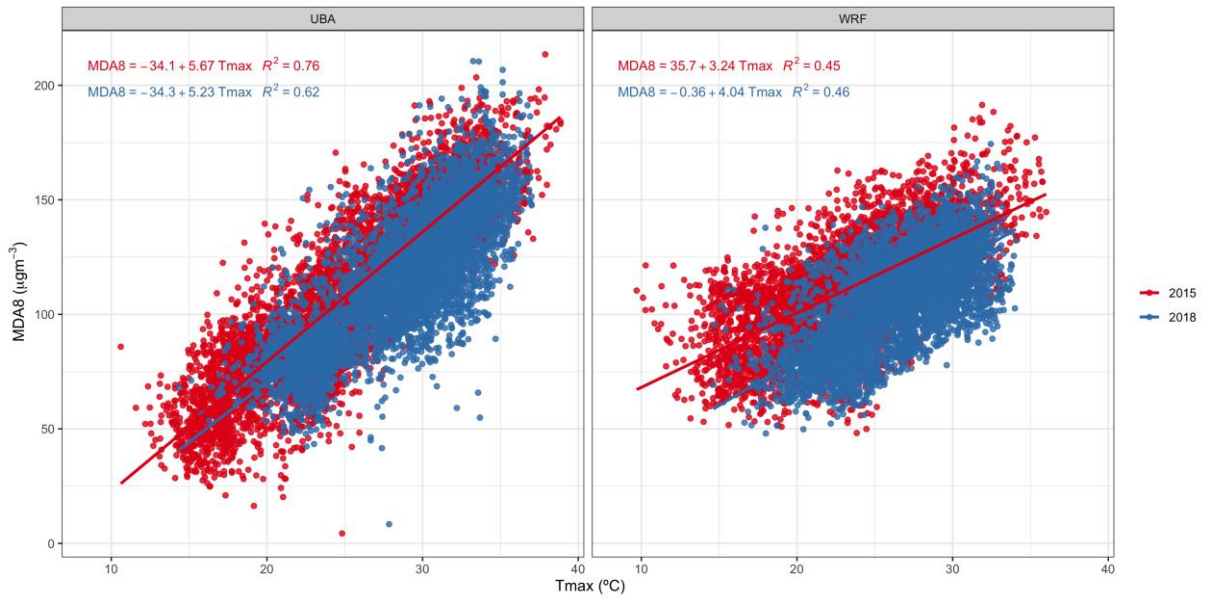
Figure 4. Scatter plots showing the MDA8 O$_3$ concentration versus the T2MAX for 2015 (red dots) and 2018 (blue dots) for all analyzed stations. The left panel depicts the observed MDA8 O$_3$ vs ERA5 T2MAX, while the right panel exhibits the modeled MDA8 O$_3$ and T2MAX. The solid lines are the lines of best fit.
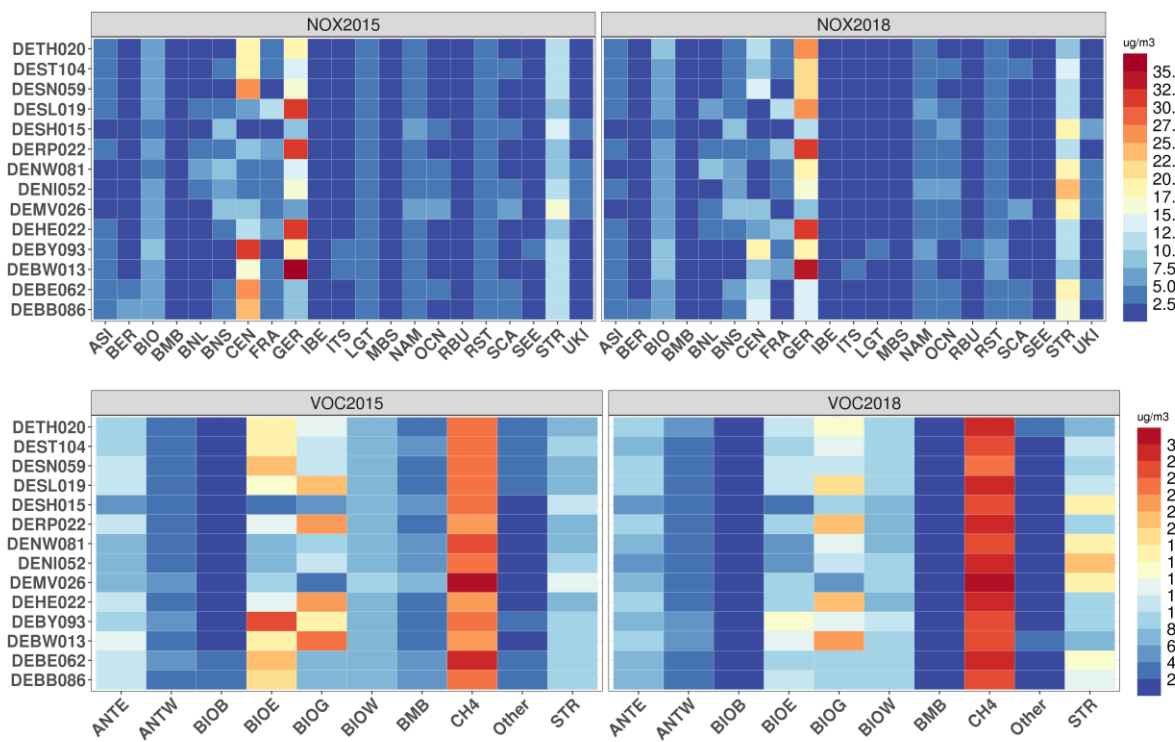
Figure 5. Contribution of NOx and VOCs precursors to mean surface O$_3$ at 14 receptor stations from local and other European sources, HTAP2 sources, and other global sources. The upper panels denote the mean contribution of NO$_x$ precursor to total O$_3$ during 6 – 13 August 2015 (left) and 1 – 8 August 2018 (right). The bottom panels denote the mean contribution of VOC precursors to total O$_3$ during 6 – 13 August 2015 (left) and 1 – 8 August 2018 (right).
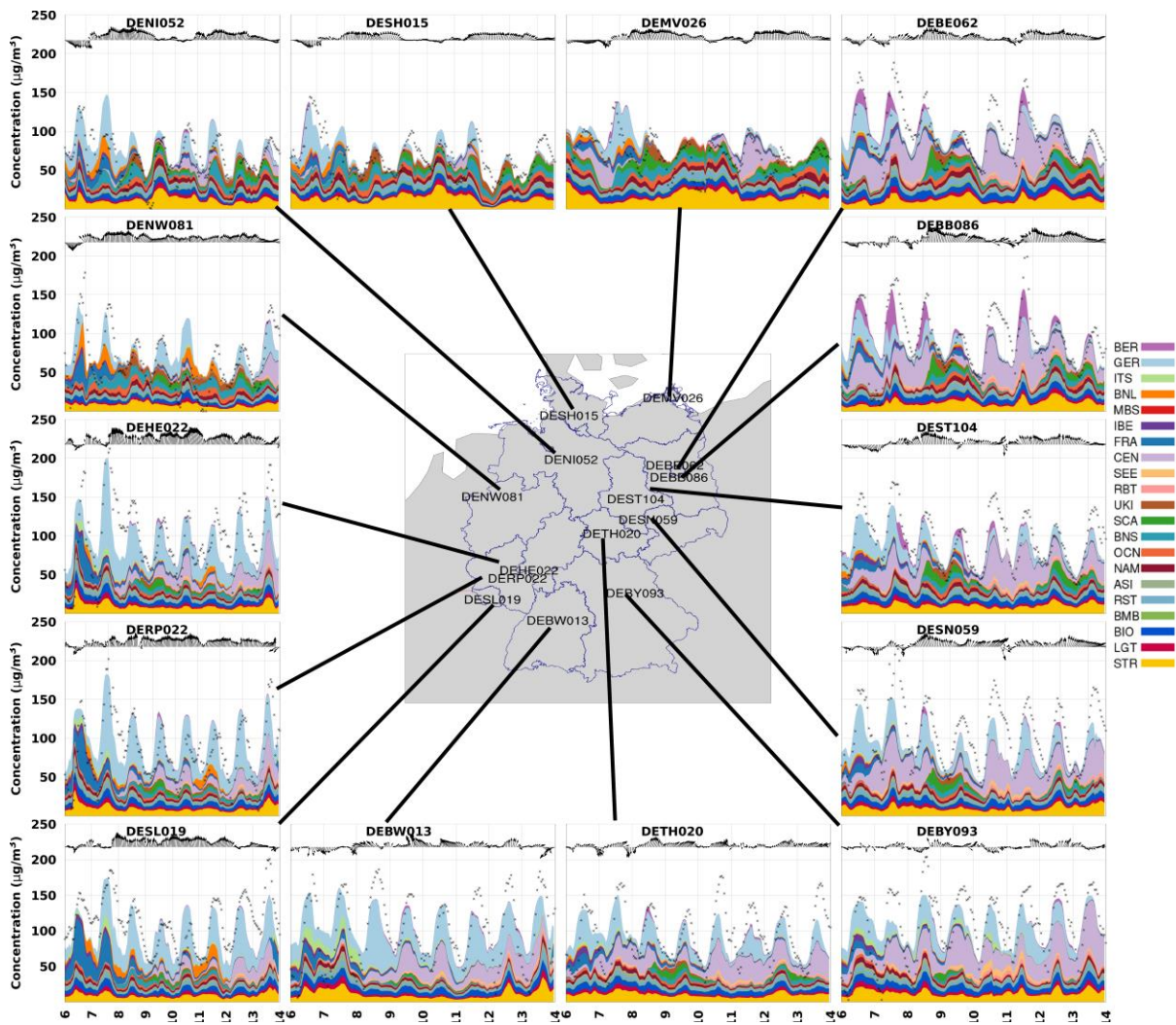
Figure 6. Contribution of regional NO$_x$ sources to hourly O$_3$ concentrations of local and other European sources, HTAP2 source regions, and other global source types at each station during the 6 – 13 August 2015 period. In addition, the vectors along the top of each panel represent the calculated wind speed and direction at 10 m above ground level. The black dots represent the observed O$_3$ concentrations.
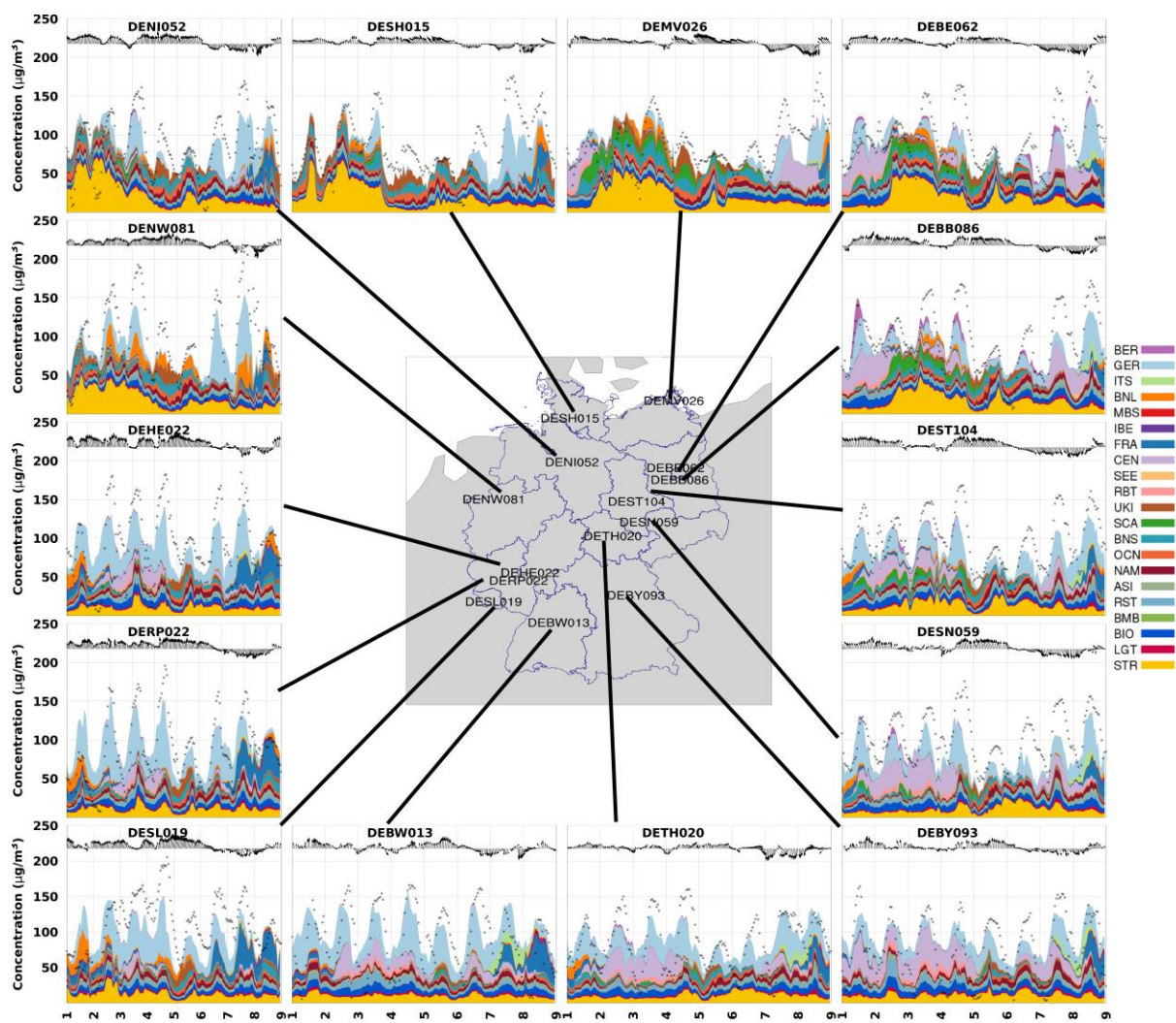
Figure 76. Contribution of regional NO$_x$ sources to hourly O$_3$ concentrations of local and other European sources, HTAP2 source regions, and other global source types at each station during the 1 – 8 August 2018 period. In addition, the vectors along the top of each panel represent the calculated wind speed and direction at 10 m above ground level. The black dots represent the observed O$_3$ concentrations.
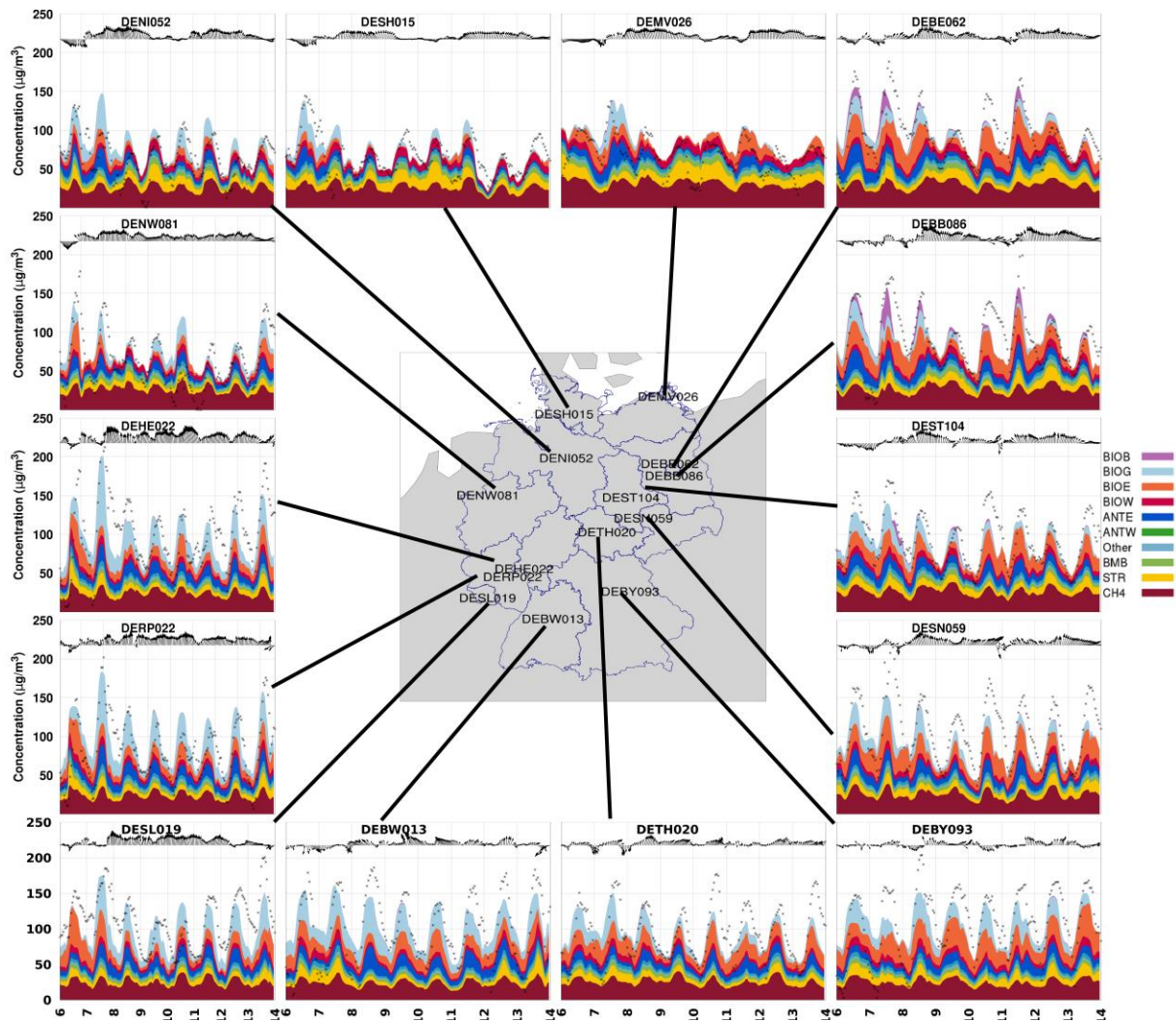
Figure 7~~8~~. Contribution of regional VOC sources to hourly O₃ concentrations of local and other European sources, HTAP2 source regions, and other global source types at each station during the 6 – 13 August 2015 period. In addition, the vectors along the top of each panel represent the calculated wind speed and direction at 10 m above ground level

Figure 98. Contribution of regional VOC sources to hourly O_3 concentrations of local and other European sources, HTAP2 source regions, and other global source types at each station during the 1 – 8 August 2018 period. In addition, the vectors along the top of each panel represent the calculated wind speed and direction at 10 m above ground level. The black dots represent the observed O_3 concentrations.
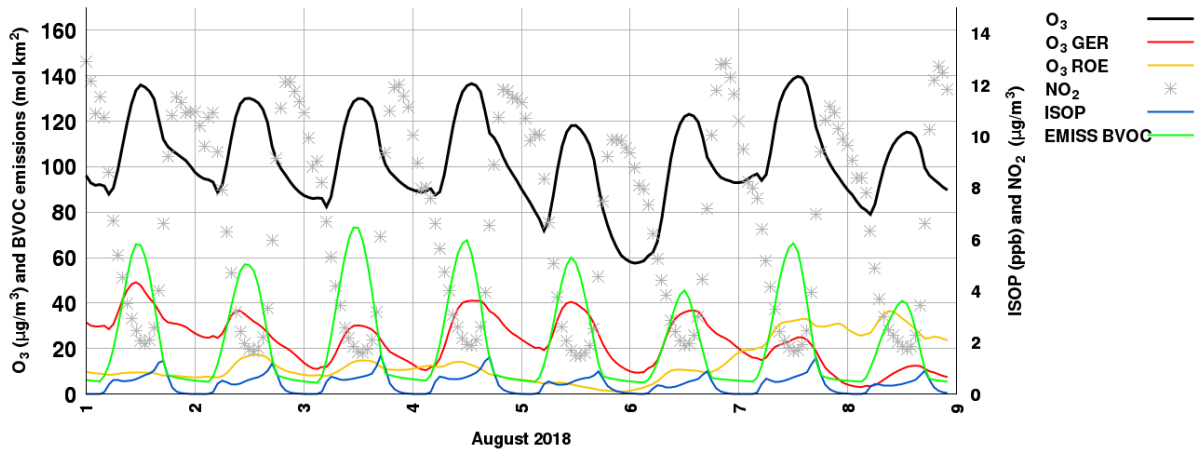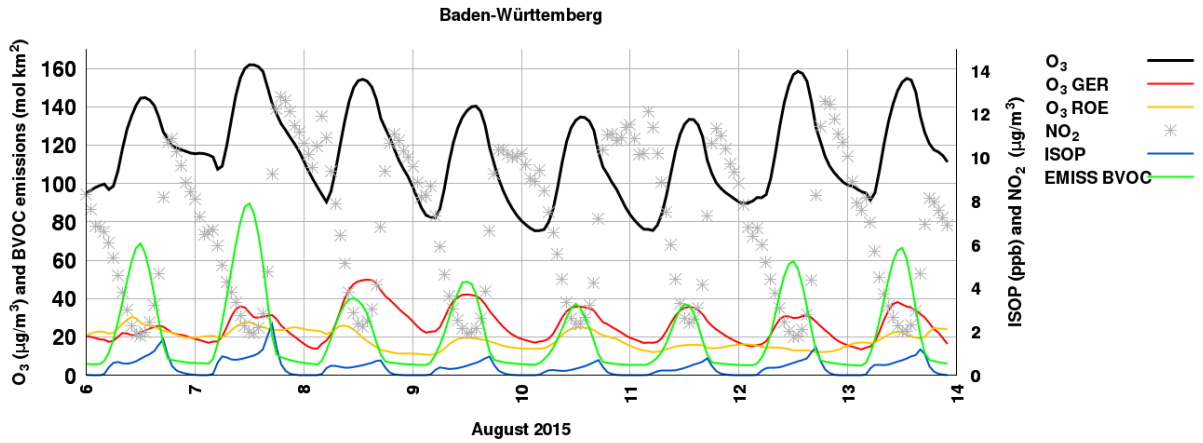
1115

Figure 109. Diurnal variation of total ozone and its German and European components together with the total BVOC emissions and isoprene concentration for 6 – 13 August 2015 (upper panel) and 1 – 8 August 2018 (lower panel)

1120